The role of manganese ore reduction morphology development in setting reduction mechanisms.

Keywords: Ferromanganese; Manganese ore; Glass phase; Reduction; Phase chemistry

Theresa Coetsee

e-mail: theresa.coetsee@up.ac.za

Department of Materials Science and Metallurgical Engineering, University of Pretoria, South Africa

Abstract

Manganese ores differ extensively in their mineralogical and bulk chemical composition. Consequently these ores follow different mineralogical morphology development paths as the reduction reaction proceeds in the production furnace. Mineralogical factors such as composition and distribution of initial liquid silicate formed at specific temperatures, as well as iron and manganese metallisation patterns, are significant determining factors in the relative importance of different parallel reduction reaction mechanisms in each ore type. Applied mineralogy techniques were used to identify and analyse matrix liquid silicate phase formation in manganese ore reacted at 1300°C with Carbon Black reductant. The study includes three South African ores from the Kalahari Manganese Field, the ores represent both the Wessels-type and Mamatwan-type mineralogy. FactSage computational thermodynamic calculations were made to explain liquid silicate phase formation and its evolution with increased reaction time. Matrix silicate phase liquidus temperatures and pseudo-ternary phase diagrams in the MnO-FeO-SiO_2-CaO-MgO-Al_2O_3 composition system were calculated. Matrix liquid silicate formed at the relatively low reaction temperature of 1300°C within all three ores, although different quantities of liquid silicate formed along differing composition paths set by ore mineralogy.

1. Introduction

Manganese ores vary widely in their mineralogical and chemical composition. The main South African manganese ores fall into two groups, carbonate containing ore (Mamatwan-type) such as Mamatwan or Gloria ore (different mines from the same ore body) or high manganese and iron-containing ores (Wessels-type) such as Wessels or Nchwaning ore, (Kleyenstüber, 1984). In most instances these ores are used to produce high carbon ferromanganese alloy (HCFeMn), which is used as an additive to steelmaking. Table I illustrates the typical chemical specifications for standard HCFeMn (ASTM A8=99-03, 2014). In order to attain the specified chemical composition of HCFeMn, two or more manganese ores are added to the SAF (Submerged Arc Furnace) feed mixture, due to the different manganese to iron ratio values within each ore. The level of raw carbonate ore in the SAF feed

mixture is limited mainly due to operational safety concerns, but also due to targeting lower electrical energy consumption by pre-calcining the ore carbonates in a sinter strand. The sinter is then fed as part of the feed mixture to the SAF.

Grade	%Mn	%C max	%Si max	%P max	%S max
A	78.0-82.0	7.5	1.2	0.35	0.05
B	76.0-78.0	7.5	1.2	0.35	0.05
C	74.0-76.0	7.5	1.2	0.35	0.05

Table I: Alloy compositions: ASTM specification for standard ferromanganese, ASTM A99-03(2014)

The heterogeneous mineralogy of manganese ores and the consequential heterogeneous reduction reaction extent in each ore have created difficulties for process metallurgists in describing manganese ore reduction to the same level of mathematical detail attained for iron ore reduction. Despite mineralogy variation amongst and in different ores, there are two to three distinct reduction stages which were identified in various laboratory studies, (Koursaris and See, 1979; Koursaris et al., 1983; Eric and Burucu, 1992; Ostrovski and Webb, 1995; Akdogan and Eric, 1995). In the rapid first reduction stage the higher oxides of manganese and iron are reduced by CO to MnO and FeO (resulting in approximately 30% reduction). In the markedly slower second stage of reduction, metallisation of FeO and MnO starts. Metallisation begins with metallic iron nucleation throughout the reduced ore particle, next to solid monoxide particles within the liquid silicate slag (glass phase). In Mamatwan ore reduction, the second reduction stage spanned the reduction range of 30%-60% at 1300°C and 30-70% at 1350°C, and was determined to be most likely under chemical reaction control for the reduction reaction of solid monoxide by CO gas to Mn_5C_2 (Eric and Burucu, 1992).

In the third stage, final reduction of MnO by carbon occurs. This stage has the lowest reduction rate (Eric and Burucu, 1992), most likely due to the slow diffusion of Mn^{2+} ions in the monoxide phase, and/or liquid silicate phase coating the monoxide phase. In the second and third reduction stages manganese is reduced from the liquid silicate phase and from the monoxide solid-solution phase, if the latter is present. The monoxide solid solution phase contains MnO and MgO, whilst lime reports to the liquid silicate phase by preference (Koursaris and See, 1979; Koursaris et al., 1983; Coetsee et al., 2015). In the South African ores considered here, only Mamatwan ore contains significant levels of MgO at 4 mass%. Therefore, the monoxide phase contains mostly MnO and therefore the MnO activity in the monoxide is close to unity. Once manganese reduction has proceeded to the extent that the monoxide phase is consumed, and only dissolved MnO in the liquid silicate phase remains, the reduction reaction slows dramatically as the MnO activity decreases (Tangstad and Olsen, 1997).

Initial metallic iron nucleation in reduced ore particles favours manganese oxide reduction by lowering the manganese activity in the initial iron-manganese alloy, (Braga et al., 2007). Thermodynamic calculations for different levels of manganese activity, at low CO_2 partial pressures, illustrated that carbothermic reduction of MnO is possible at temperatures as low as 1250°C, compared to 1403°C required at unit activities, (Coetsee, 2018). Therefore, manganese ore with higher iron oxide content which is closely associated with manganese in the same mineral phase should result in faster ore reduction rates, at least initially before liquid silicate phase forms to hinder gas access to iron oxides in the reduced ore particle. The more critical phase chemistry parameters are liquid silicate formation

temperature and its MnO saturation level, because these factors will determine the onset of stage three reduction for each ore, and the extent of hindrance of gas access to oxides within the reduced ore particle, (Coetsee, 2018). Alternative processing options for high and low grade manganese ores (Ferruginous) also involve account of silicate glass formation for different processing aims and limits. In manganese ore reduction with methane containing gas, formation of liquid silicate glass may hinder methane gas access to the ore particle interior and so set an upper limit on the process temperature, (Ostrovski et al., 2004; Liu et al., 2018). Silicate glass formation is also of importance in the direct reduction of Ferruginous ores followed by magnetic separation of metallic iron particles to upgrade the Mn/Fe content of the non-magnetic fraction. Sodium salts are added prior to reduction at 1100°C to destroy the ferro-tephroite structure to promote FeO reduction to metallic iron, and to facilitate metallic phase volume growth for better subsequent magnetic separation from the non-magnetic fraction of MnO and sodium-silicate, (Liu et al., 2019). Another processing option used for Ferruginous ores utilisation is sintering of ore fines in which bonding phase formation was found to be silicates in the form of ferro-tephroite and Ca-Al-Mn-Fe-silicate, (Zhang et al., 2016).

Liquid silicate phase formation and its composition were identified in previous studies on the reduction of individual South African manganese ores (Koursaris et al., 1983; Eric and Burucu, 1992; Akdogan and Eric, 1995). However, theses studies focused on the overall reduction process and therefore liquid silicate analyses were co-incidental and few in number and the experimental conditions were not set to specifically measure liquid silicate phase formation. For example Koursaris et al. (1983) reacted 20mm sized cubes of Mamatwan ore surrounded by reductant for one to three hours at temperatures ranging from 1200°C to 1500°C under Argon gas and identified the liquid silicate phase as $(Ca,Mn)_2SiO_4$ containing also FeO and MgO, without providing detailed SEM analyses. Eric and Burucu (1992) reacted milled calcined Mamatwan ore under Argon gas with graphite powder at 1100°C to 1350°C for reaction times of 6 to 90 minutes and reported earliest liquid silicate formation at 10 minutes reaction time at 1350°C in one SEM analyses point. In a similar study of three different grades of Wessels ore, Akdogan and Eric (1995) reported liquid silicate formation at 1300°C at 8 minutes, 20 minutes and 30 minutes reaction time. Even in the basence of large quantities of gangue components which may facilitate silicate glass formation, it was shown that a small quantity of silica added to pure MnO (2.5 mass%) caused a lowered reduction rate of MnO with graphite at 1350°C due to formation of molten ß-$MnSiO_3$, (Rankin and Van Deventer, 1980; Van Deventer, 1987).

Therefore, the two mineralogical aspects, which take place in the initial stages of manganese ore reduction, seem to have large influences in the overall reduction mechanisms and resultant kinetics of manganese ore reduction: the distribution of initial metallic iron prills and beads formed in the reduced ore particles, and initial liquid silicate (glass phase) formation in the second stage of reduction. Applied mineralogy is required to investigate these two aspects because bulk chemistry and thermodynamic phase chemistry calculations are not able to accurately predict phase morphology development in manganese ore reduction. The objective of this study is to investigate reduced ore phase chemistry and phase distribution and use this information to to better explain differences in reduction rate variation among South African ores of the carbonate type (Mamatwan) and the high

manganese and iron content type (Nchwaning and Wessels). FactSage 6.4 thermochemical software is used to interpret liquid silicate phase chemistry evolution as a function of increased reaction time, and to calculate silicate phase liquidus temperatures because experimentally determined four and five component phase diagrams in the CaO-MnO-SiO_2-MgO-FeO system are not available from literature.

2. Methods and Materials

Three manganese ores were individually reacted in reduction experiments: Mamatwan, Nchwaning and Wessels ore of -2.8 mm +1.4 mm. Ore bulk chemical analyses (Table II) included major element analyses by XRF (X-ray fluoresence) using an ARL Advant'X Series Sequential XRF Intellipower instrument from ThermoFisher Scientific, moisture content analysis and carbon and sulfur content analysis by combustion method using a Leco CS230SH instrument from LECO. Carbon Black powder (-200 µm) was used as the reductant. The carbon ultimate analysis (C, H, N, S, O) was done by combustion (LECO) analysis method (Table III).

	Mamatwan	Nchwaning	Wessels
SiO_2	6.1	8.0	2.8
Al_2O_3	0.2	0.3	0.4
FeO*	6.3	13.3	15.8
CaO	13.9	3.5	4.9
MgO	4.0	0.6	0.4
K_2O	0.01	0.01	0.07
MnO*	49.8	64.8	61.6
P	0.02	0.03	0.04
S	0.03	0.10	0.09
Ba	0.1	0.3	0.9
Na_2O	0.04	0.04	1.03
Moisture	0.03	0.10	0.09
C	4.38	0.50	0.21
Total	84.8	91.1	88.2
Mn	38.5	50.2	47.7
Fe	4.9	10.3	12.3
Mn/Fe	7.9	4.9	3.9
LOI	15.9	3.5	5.2
B2	2.3	0.4	1.8
B3	2.9	0.5	1.9

B2=%CaO/%SiO_2; B3=(%CaO+%MgO)/%SiO_2; *Total iron expressed as FeO; **Total manganese expressed as MnO

Table II: Manganese ore bulk chemical composition (mass%)

	mass%
C	96.1
H	0.44
N	0.13
O	<0.1
S	1.64
Moisture	0.65
Ash	1.03

Table III: Carbon Black bulk composition (mass%)

Ore mineral composition was determined by XRD (X-ray diffraction) using a PANalytical Aeris diffractometer with PIXcel detector and fixed slits with Fe filtered Co-Kα radiation with a special PHD setting for fluorescent material. Mineral phases were identified using X'Pert Highscore plus software. The relative phase amounts (mass%) were estimated by using the Rietveld method. The Rietveld quantification goodness of fit parameter was 1.05 to 1.69 across raw ore and reacted ore samples. XRD analyses detection limit was 0.5-3 mass%, therefore XRD analyses numbers were rounded up to whole numbers. Sample preparation included addition of 20 mass% silicon metal as internal crystalline standard to the sample, and micronizing in a McCrone micronizing mill. Since only the crystalline phases are quantified in the Rietveld method, the mass% crystalline phases is over-estimated in the XRD analysis due to the presence of amorphous phase in the sample (which is invisible in the XRD analysis). The 20 mass% silicon metal added as internal standard will also be proportionally over-estimated due to the presence of the amorphous phase and this over-estimation proportion allows for back-calculation of the mass% amorphous phase present in the sample. Amorphous phase mass% quantification error from calculation and weighing errors was estimated to be ±10-15 mass%. Substantial amounts of amorphous phase were identified in all the reacted samples, which also included the amorphous Carbon Black reductant (confirmed from a separate Carbon Black sample XRD scan).

The main mineral phases identified within each ore (Table IV) were Braunite, Diopside, Kutnohorite and Hausmanite in Mamatwan ore; Braunite and Hematite in Nchwaning ore and Braunite, Bixbyite, Manganite and Hematite in Wessels ore. The similarity in XRD patterns among Braunite sub-types made clear distinction between these mineral phases difficult. However, it is well described in literature that Braunite I presents in Mamatwan type ore and Braunite II in Wessels type ore, (Kleyenstüber, 1984; Chetty and Gutzmer, 2018).

Mineral phase	Mamatwan	Nchwaning	Wessels
Braunite I ($Mn^{2+}Mn_6^{3+}SiO_{12}$)	37	87	2
Braunite II ($CaFe_{2.38}Mn_{11.62}SiO_{24}$	nd*	nd	36
Bixbyite (Mn_2O_3)	nd	nd	21
Calcite ($CaCO_3$)	2	2	nd
Diopside, manganoan ($Ca_{0.87}Mg_{0.94}Mn_{0.19})Si_2O_6$	25	nd	nd
Hausmanite (Mn_3O_4)	14	nd	nd
Hematite (Fe_2O_3)	nd	11	16
Jacobsite ($Fe_2^{3+}Mn^{2+})O_4$	1	nd	nd
Johannsenite ($CaMnSi_2O_6$)	nd	nd	3
Kutnohorite $Ca(Fe_{0.13}Mg_{0.23}Mn_{0.64})(CO_3)_2$	18	nd	nd
Lizardite ($H_4Mg_3Si_2O_9$)	3	nd	nd
Manganite (MnO.OH)	nd	nd	22

*nd=not detected

Table IV: Ore minerals from XRD analysis (mass%)

Reductant addition requirement for each ore was calculated by mass balance for total metallisation of manganese and iron assuming all elements are contained as oxides. For manganese, iron, magnesium and calcium, the following mineral expressions were used to calculate the carbon requirement for each ore: in Mamatwan ore: Braunite I ($Mn^{2+}Mn_6^{3+}SiO_{12}$), Calcite ($CaCO_3$), Magnesite

($MgCO_3$) and Hematite (Fe_2O_3), in Nchwaning and Wessels ore: Hematite (Fe_2O_3), Bixbyite (Mn_2O_3) and Calcite ($CaCO_3$) to satisfy the level of carbon analysed in the ore. The following reduction parameters were used for the carbon requirement calculation: product gas in the calculation was 100%CO and therefore included the regeneration carbonate calcination CO_2 to CO, and carburisation of the alloy to 8%C.

The level of carbon requirement is expressed as the mol ratio of carbon to reducible oxygen (C/O) to meaningfully present the importance of carbon addition, as compared to a mass% carbon addition number. In the (C/O) value, reducible oxygen (O) is the sum of the moles of oxygen associated with Mn and Fe oxides and C is the mole carbon added to the mixture, based on the ultimate analysis in Table III. Due to high levels of carbonates present in Mamatwan ore, as compared to Nchwaning and Wessels ore, the C/O in Mamatwan mixture is higher at 1.6 vs. 1.3 for Nchwaning and Wessels mixtures. The absolute elemental carbon requirement values are similar at 17 mass% C vs. 20 mass% C. Therefore, in all of the experiments the level of Carbon Black addition was 20 mass% (which is equivalent to 19 mass% C).

Mixtures of manganese ore and graphite reductant were reacted in carbon steel crucibles under Argon gas in a muffle furnace at 1300°C for 10, 20 and 30 minutes. Upon completion of the reaction time the crucible was removed from the furnace and cooled under Argon gas. Each starting sample mixture contained 40 grams of ore and 10 grams of carbon black. Polished sections were prepared from the reacted mixtures to study reduced ore particle phase morphology and chemistry by methods of light optical microscopy at x50 magnification (Olympus BX51M) and Scanning Electron Microscopy (SEM) using a JEOL-IT300 SEM-EDS with Oxford X-max 50 detector. Element analyses from individual sample phase areas were made at 15kV and 60 seconds count time. The maximum element analyses one sigma error was 0.44 mass%. The presence of oxygen in the phase SEM-EDS element analysis served as identifier for oxide phases. The metal cation element analyses were expressed as MnO, FeO, SiO_2, CaO, MgO, Al_2O_3. Back-scattered electron (BSE) images were collected for phase illustration purposes. The BSE image in Figure 1 illustrates the application of SEM-EDS spectrum analyses with oxygen in combination with BSE gray scale levels to distinguish between oxide phases (gray) and alloy (white).

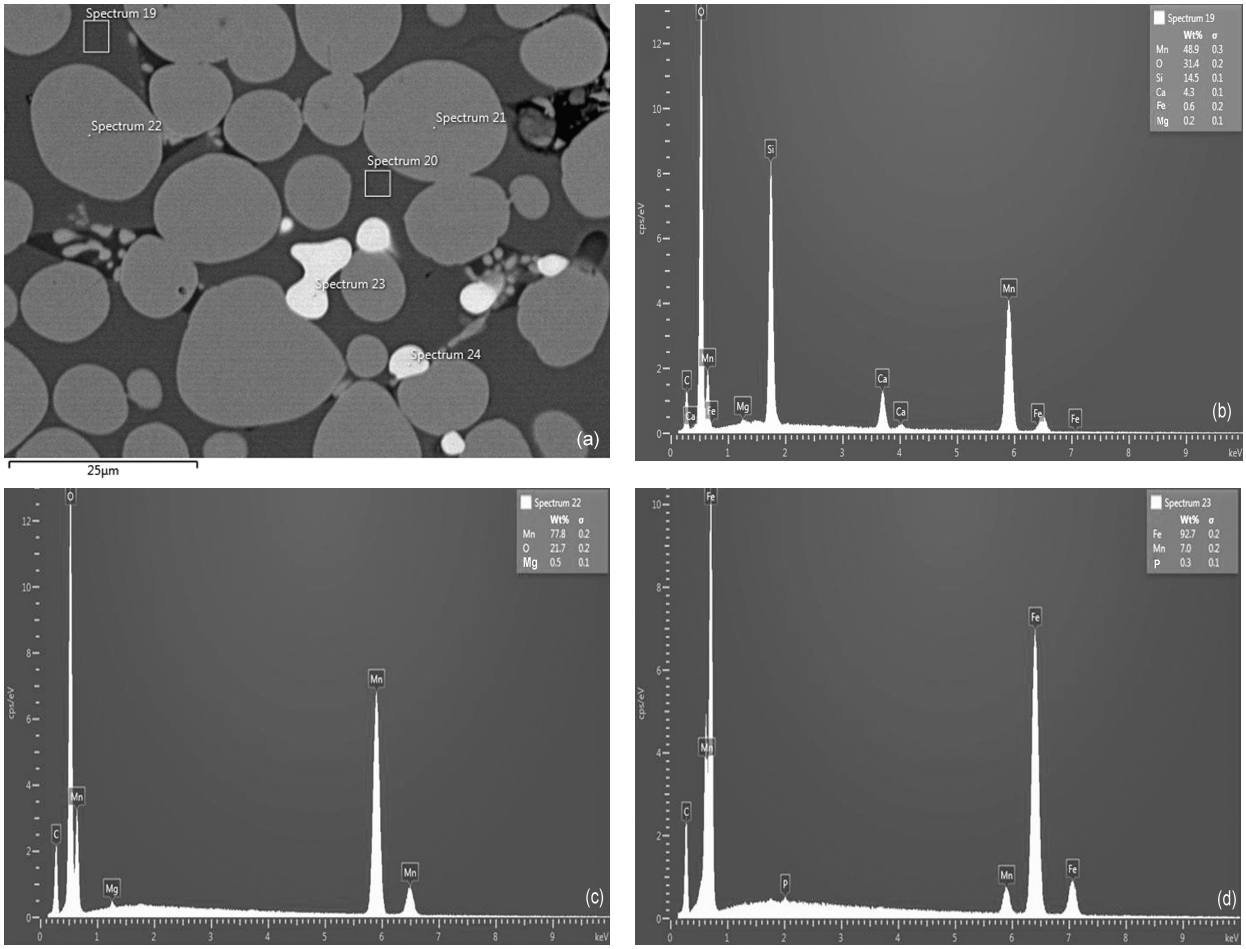

Figure 1: (a) BSE image (x1600) of Nchwaning ore reacted for 30 minutes at 1300°C (b) Area 19 EDS spectrum for silicate (dark gray) (c) Area 22 EDS spectrum for monoxide (light gray) (d) Area 23 EDS spectrum for alloy (white)

The Equilib module in FactSage 6.4 (with the FTOxid database) was used to calculate liquidus temperatures of the silicate glass phase compositions measured by SEM analyses. Appendix A contains the individual silicate glass phase SEM analyses as entered into the Equilib module, and the outputs from this module calculation as the liquidus temperature and primary solidification phase for each glass analysis. Silicate glass phase liquidus compositions were projected onto relevant pseudo-ternary phase diagrams calculated in the Phase diagram module of FactSage 6.4 (FTOxid database) to better display glass phase compositions trends. In order to plot individual glass phase analyses as summarised in Appendix A onto MnO-FeO-SiO_2-CaO-MgO-Al_2O_3 pseudo-ternary phase diagrams, the minor components in the glass phase analyses from Appendix A, mass% FeO and mass% MgO, were forced to chosen levels as displayed in the pseudo-ternary phase diagram captions. The following solution phases were selected in all Equilib module and Phase diagram module calculations: ASlag-liq all oxides+S, AMonoxide, Orthopyroxene, AWollastonite, a'Ca_2SiO_4, a-Ca_2SiO_4, Mellilite, AOlivine, M_2O_3(Corundum), Mn_2O_3(Bixbyite), Mn_7SiO_{12}, Rhodonite.

3. Results and discussion

Reacted sample mixture XRD patterns at increased reaction time are illustrated in Figures 2-4. For each ore at each reaction time the main crystalline phase formed was Manganosite (MnO). Very little, if any unreacted ore minerals were identified in the reacted sample XRD analyses, even for samples reacted for 10 minutes. All of the reacted samples contained metallic iron which was confirmed in optical microscopy observations and by SEM analyses as Mn-Fe alloy. A Fayalite type phase was identified in all of the Nchwaning reacted sample XRD analyses. The limited information gleaned from XRD patterns in Figures 2-4 necessitated further investigation of the reacted sample mineralogy. Therefore, polished sections were analysed by the SEM (Scanning Electron Microscopy) to identify the specific glass phase chemistries.

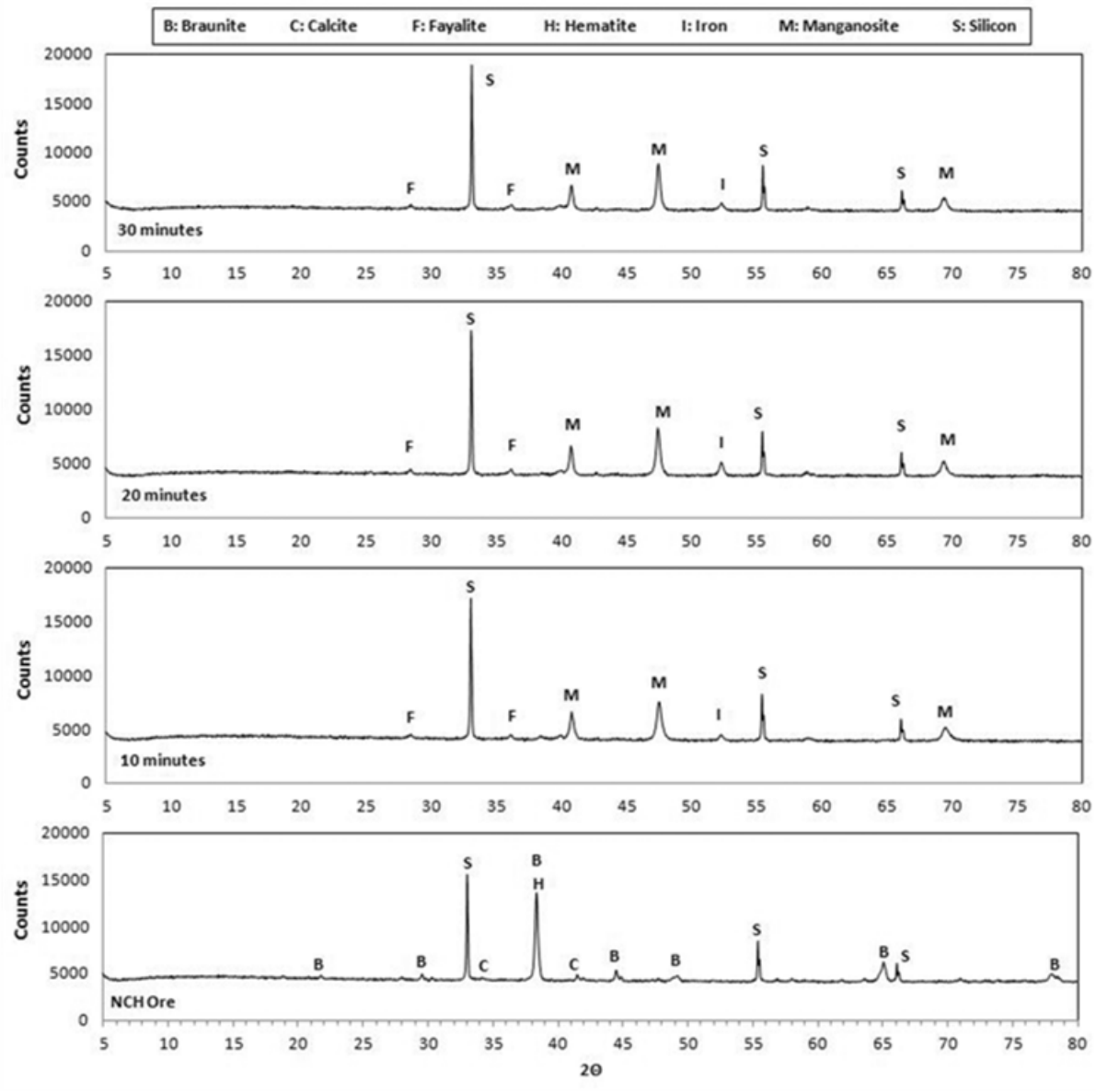

Figure 2: XRD analyses for Nchwaning ore and Nchwaning-reductant mixtures reacted for 10, 20 and 30 minutes.

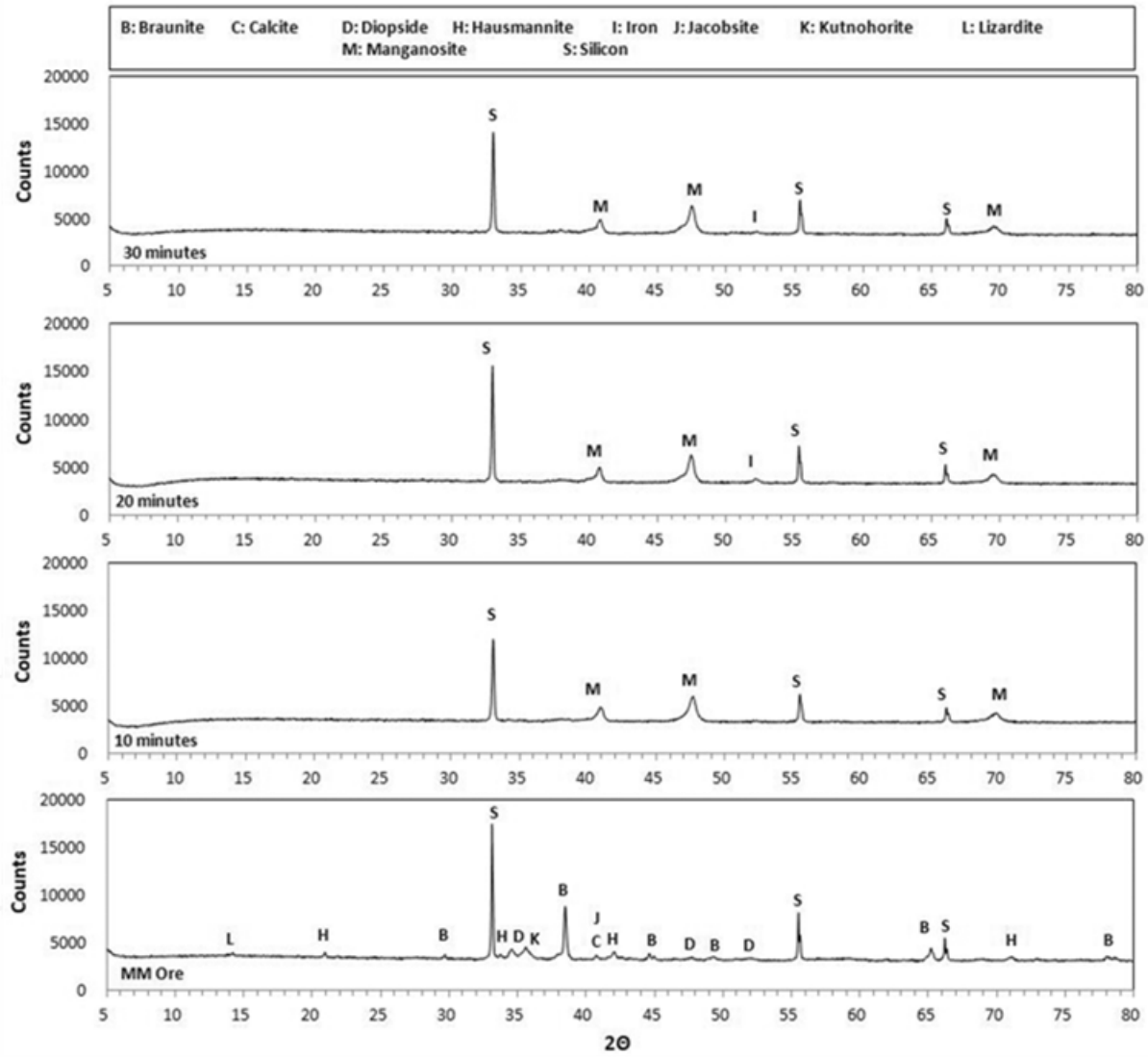

Figure 3: XRD analyses for Mamatwan ore and Mamatwan-reductant mixtures reacted for 10, 20 and 30 minutes.

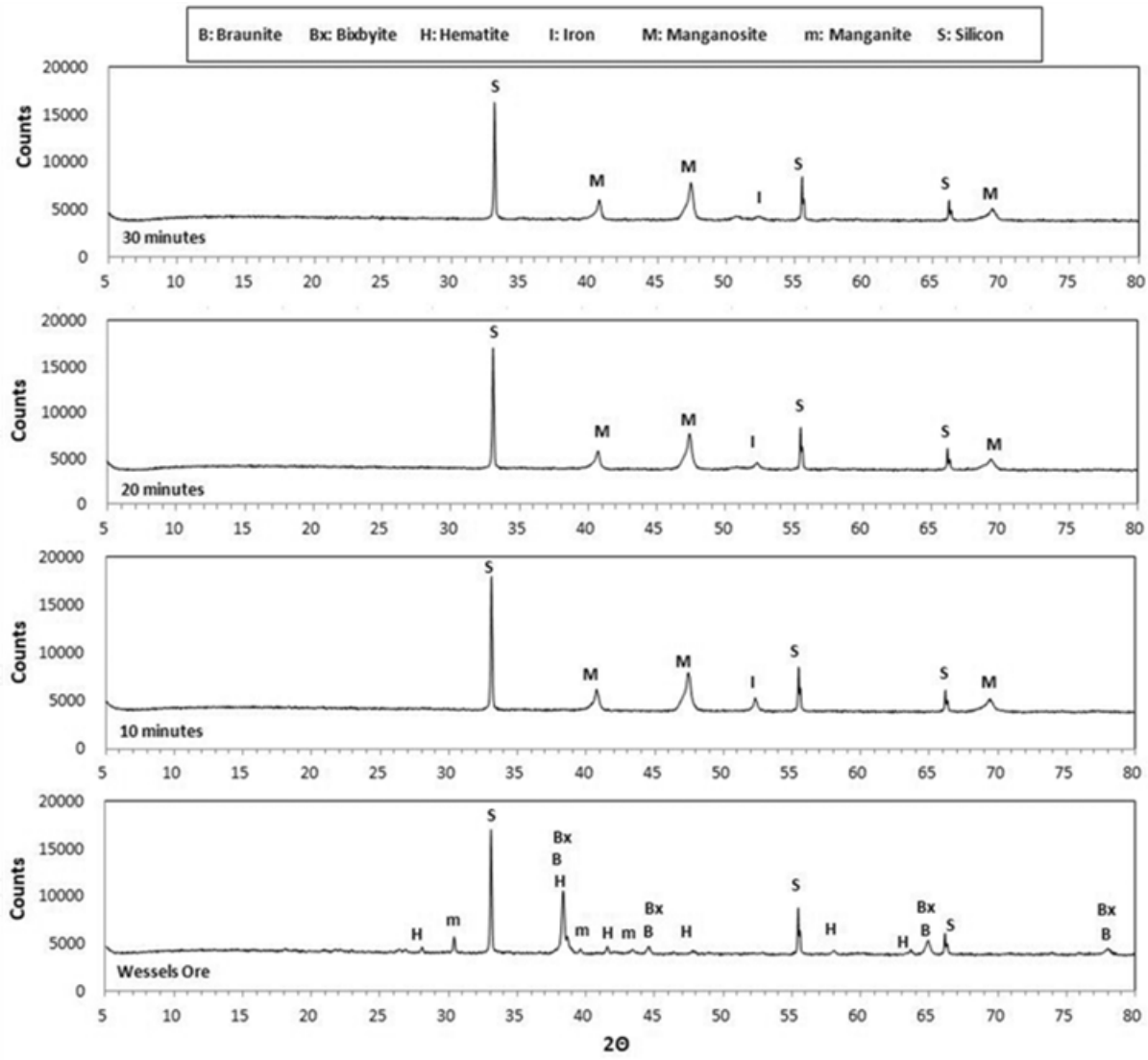

Figure 4: XRD analyses for Wessels ore and Wessels-reductant mixtures reacted for 10, 20 and 30 minutes.

Photomicrographs in Figures 5-7 illustrate extensive variation in metallisation patterns in reduced particles within the same ore. Metal prills in reduced Mamatwan ore (Figure 6) appear much smaller compared to metal prills contained in reduced Nchwaning ore (Figure 5) and Wesses ore (Figure 7). However, metal prills in reduced Mamatwan ore appear more evenly distributed, compared to metal prills and beads in reduced Nchwaning and Wessels ores. Matrix glass phase appear in all of the particles in Figures 5-7, although larger magnification is required in some instances to view the glass phase.

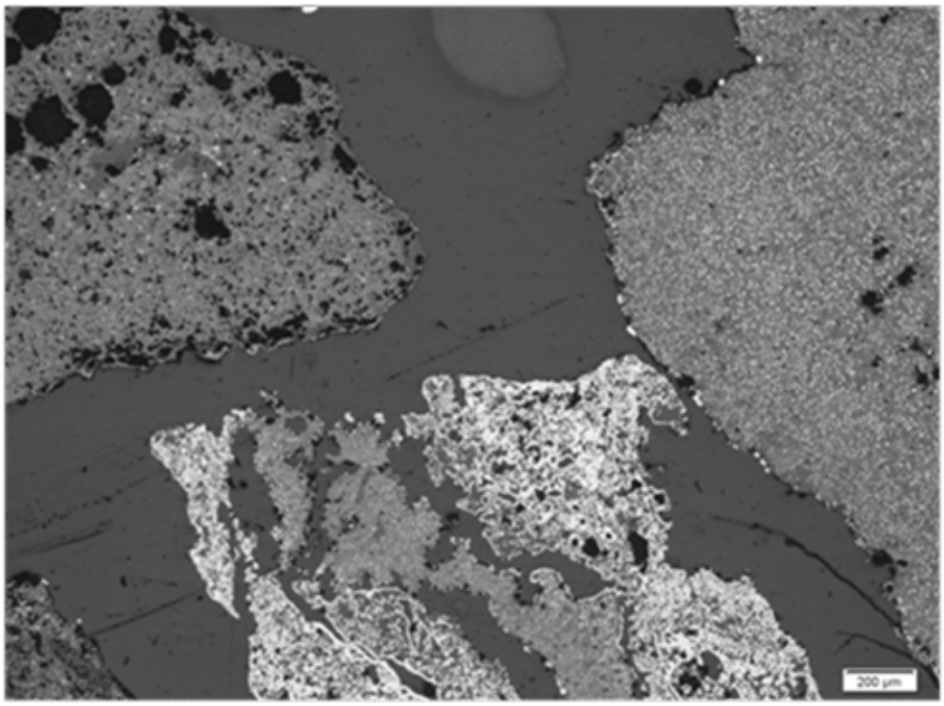

Figure 5: Photomicrograph (x50) of Nchwaning ore reacted for 20 minutes at 1300°C (light grey=monoxide, white=alloy, dark gray background phase=glass phase)

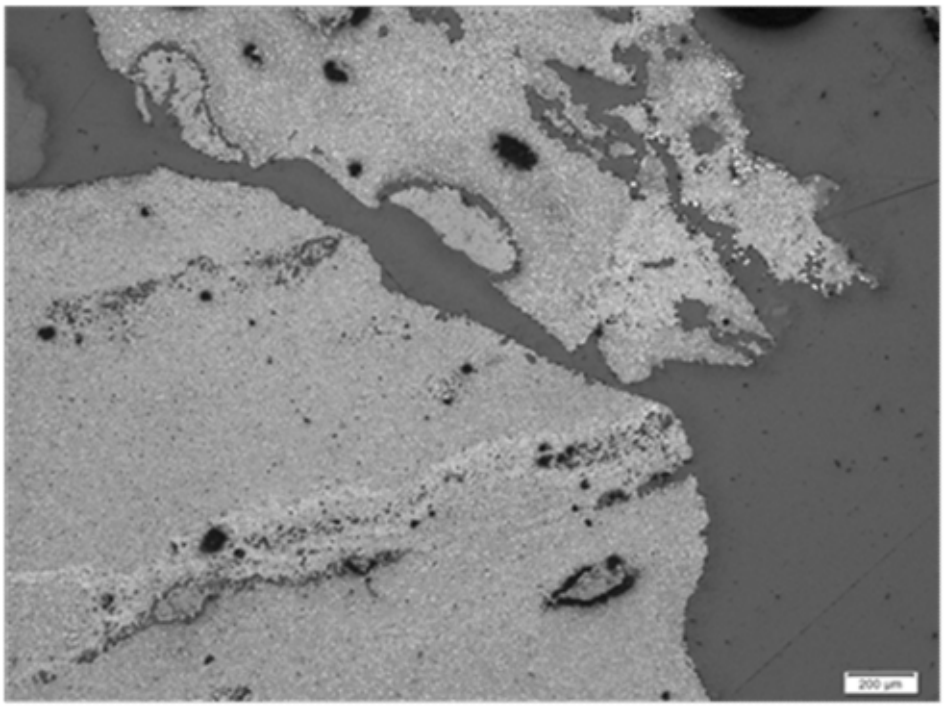

Figure 6: Photomicrograph (x50) of Mamatwan ore reacted for 20 minutes at 1300°C (light gray=monoxide, white=alloy, dark gray background phase=glass phase)

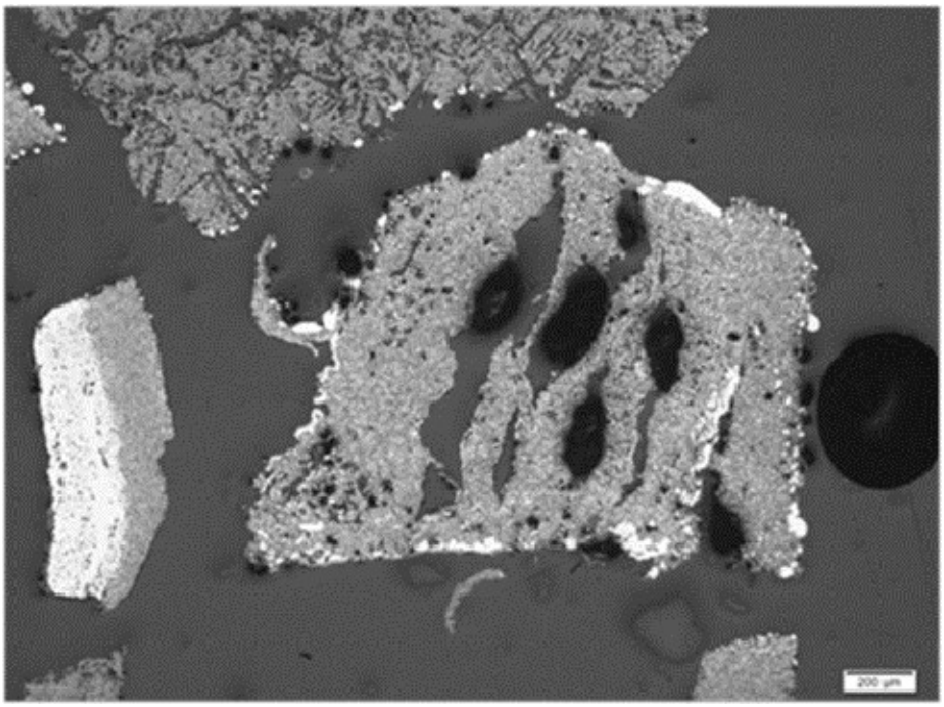

Figure 7: Photomicrograph (x50) of Wessels ore reacted for 20 minutes at 1300°C (light gray=monoxide, white=alloy, dark gray background phase=glass phase)

Figures 8-10 illustrate typical glass phase appearance within Nchwaning reduced ore particles. Associated SEM phase analyses are summarised in Table 5-7. Due to the heterogeneous reaction behaviour of the ore, some particles were reduced more extensively than others. However, examples of glass phase formation were readily found in reduced ore particles reacted for 10 minutes. Glass phase formation was observed in association with monoxide phase (Manganosite containing cations of Fe, Mg, Ca), and mostly also in association with alloy phase areas, although the quantity of associated alloy phase varied widely as is illustrated in Figures 8-10. In Nchwaning ore reacted for 10 minutes, the glass phase still contained unreacted FeO, up to 5 mass%, whilst less than 1 mass% FeO remained in glass areas at 30 minutes reaction time, as summarised in Appendix A, Table A.I.

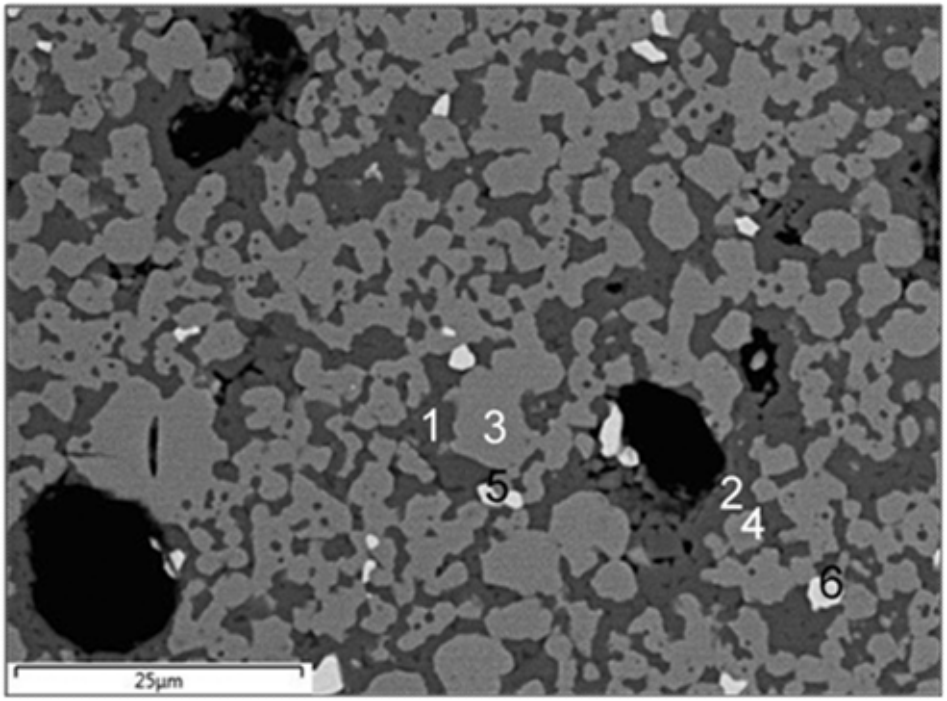

Figure 8: BSE image (x1600) of Nchwaning ore reacted for 10 minutes at 1300°C

	1	2	3	4	5	6
	glass	glass	monoxide	monoxide	alloy	alloy
CaO	2.8	3.0	0	0		
FeO	2.8	3.2	8.0	8.1		
MnO	64.5	64.3	92.0	91.9		
SiO_2	29.6	29.5	0	0		
MgO	0.2	0.0	0	0		
Mn					8 .1	3.1
Fe					91.9	96.9
Total	100	100	100	100	100	100
B2	0.1	0.1				
B3	0.1	0.1				
TL (°C)	1326	1320				

Table V: SEM analyses (mass%) of phases in Figure 8 for Nchwaning ore reacted for 10 minutes at 1300°C (TL=liquidus temperature)

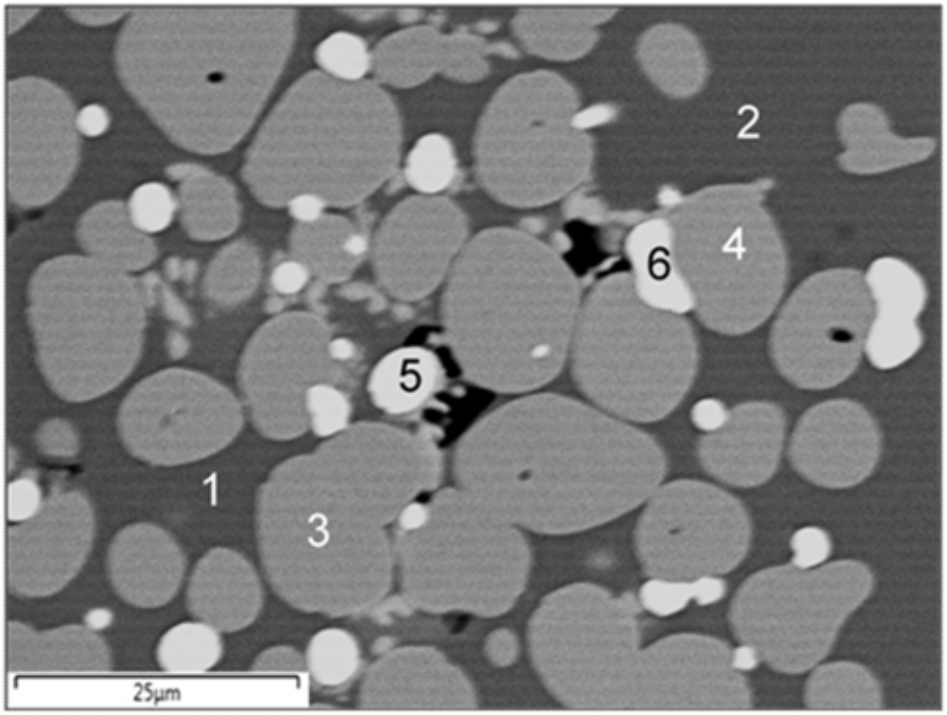

Figure 9: BSE image (x1600) of Nchwaning ore reacted for 20 minutes at 1300°C

	1	2	3	4	5	6
	glass	glass	monoxide	monoxide	alloy	alloy
CaO	3.9	3.2	0	0		
FeO	0	0.9	0	1.3		
MnO	65.6	65.7	100.0	98.7		
SiO_2	30.5	30.2	0	0		
MgO	0	0	0	0		
Mn					3.1	8.0
Fe					96.2	91.7
P					0.7	0.3
Total	100	100	100	100	100	100
B2	0.1	0.1				
B3	0.1	0.1				
TL(°C)	1326	1325				

Table VI: SEM analyses (mass%) of phases in Figure 9 for Nchwaning ore reacted for 20 minutes at 1300°C (TL=liquidus temperature)

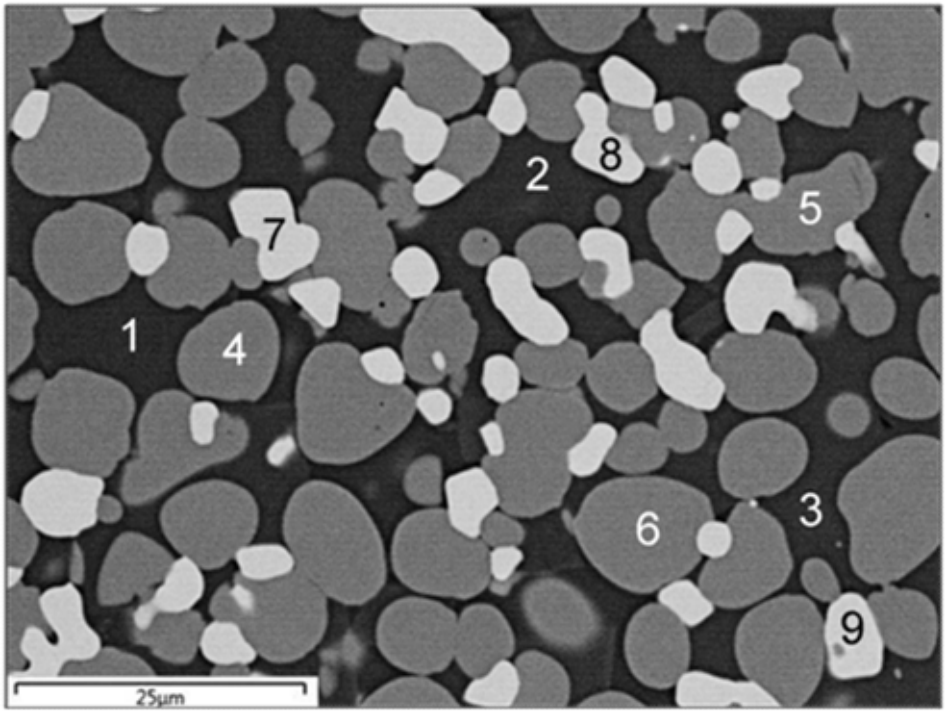

Figure 10: BSE image (x1600) of Nchwaning ore reacted for 30 minutes at 1300°C

	1	2	3	4	5	6	7	8	9
	glass	glass	glass	monoxide	monoxide	monoxide	alloy	alloy	alloy
CaO	13.4	12.0	12.5	0.3	0.3	0.3			
FeO	0	1.0	1.0	0	1.3	0			
MnO	53.8	58.5	53.9	99.0	97.9	99.0			
SiO_2	31.8	27.6	31.5	0	0	0			
MgO	1.0	0.9	1.0	0.7	0.5	0.7			
Mn							9.7	9.8	9.2
Fe							90.3	90.2	90.8
Total	100	100	100	100	100	100	100	100	100
B2	0.4	0.4	0.4						
B3	0.5	0.5	0.4						
TL(°C)	1287	1361	1289						

Table VII: SEM analyses (mass%) of phases in Figure 10 for Nchwaning ore reacted for 30 minutes at 1300°C (TL=liquidus temperature)

In the reacted Nchwaning ore, the glass phase chemistry as summarised in Appendix A, Table A.I, progressed from low lime content compositions at 10 minutes reaction time (up to 6%CaO), towards higher levels of lime content at 20 and 30 minutes reaction time (up to 41%CaO). Generally the glass phases contained low levels of MgO (<1%). In Nchwaning ore reacted for 10 minutes, glass phase basicity levels remained at low levels (B2, B3 < 0.25) compared to bulk ore basicity of B2=0.4 and B3=0.5 (Table II). The glass basicity shifted to higher levels with reaction times of 20 and 30 minutes, as displayed in Figure 11.

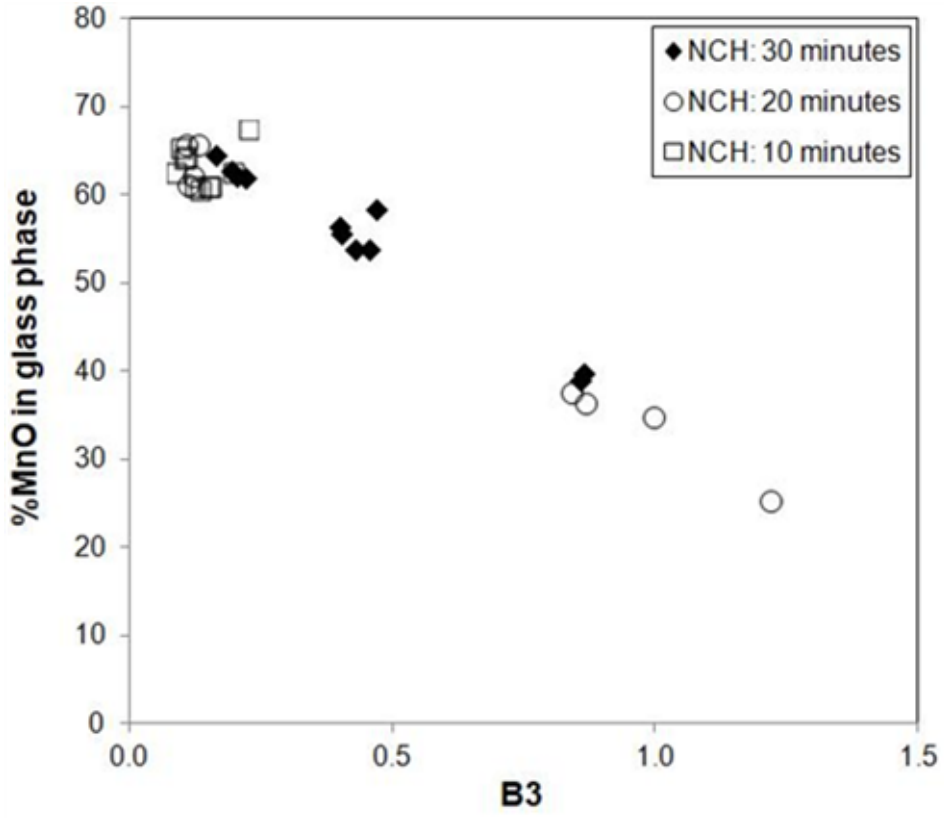

Figure 11: %MnO vs. B3 for glass phase compositions in Nchwaning ore reacted for 10, 20 and 30 minutes at 1300°C

The glass compositions in Nchwaning ore are displayed in the phase diagrams in Figures 12 and 13. Liquidus isotherms at 1300°C and 1400°C are included as reference lines. The five component system of CaO-MnO-SiO_2-1%MgO-3%FeO in Figure 12 contains the glass phase chemistry in Nchwaning ore reacted for 10 minutes at 1300°C, following adjustment of the analysed compositions to 1%MgO and 3%FeO. Prior sensitivity runs in the Equilib module of FactSage 6.4 confirmed that FeO fluxed the glass phase liquidus temperatures (20°C decrease for 5%FeO addition), and MgO increased the glass phase liquidus temperature (15°C increase for 1%MgO). Small quantities of MgO and FeO in the glass phase should not be excluded in the phase diagram plots, therefore the glass analyses for this sample was adjusted to the selected values of 1%MgO and 3%FeO to enable a comparative plot of this data set. Most of the points in Figure 12 are clustered together near the 1300°C isotherm, within the Olivine phase area, and thus in agreement with the Fayalite phase stoichiometry identified in the XRD analyses in Figure 2. Glass compositions for 30 minutes reaction time and some of those for 20 minutes reaction time are illustrated in Figure 13. The chemistry shift from initially acidic high MnO glass compositions to more basic MnO-SiO_2-CaO glass of lower MnO content is evident when the glass composition points in Figures 12 and 13 are compared. In some instances this chemistry shift resulted in even lower glass liquidus temperatures compared to the initial glass phases formed at 10 minutes reaction time. For example, in Table A.I, glass analyses 8 and 9 at 30 minutes reaction time have liquidus temperatures of 1251°C and 1260°C due to increased

levels of lime (27% CaO), lower than glass phase liquidus temperatures calculated for 10 minutes reaction time (~1320°C).

Initially formed silicate glass phase consists of Olivine-type silicate with co-ordination of $2(Mn,Ca,Mg,Fe)O.SiO_2$, and has a composition close to $2MnO.SiO_2$ (tephroite) which is in agreement with the presence of Braunite mineral phase ($Mn^{2+}Mn_6^{3+}SiO_{12}$) forming MnO and tephroite upon reduction of Mn^{3+} to Mn^{2+}, (Slag Atlas, 1995). With increased reaction time, the Olivine-type glass phase shifts in composition to higher levels of CaO as minor minerals containing CaO are assimilated into the initial liquid Olivine-type glass phase. Comparison of Figure 12 and 13 shows that the silicate glass phase composition changes with reaction time along the composition line between the $2MnO.SiO_2$ composition point towards the $2CaO.SiO_2$ composition point, until the bulk ore basicity level is reached at B2=0.4 (70%SiO_2-30%CaO) where most of the 30 minute glass phase icons in Figure 13 are grouped together. In all of the SiO_2-CaO-MnO based pseudo-ternary diagrams discussed here (Figures 12, 13, 18, 23 and 24) the level of MnO dissolved in silicate glass phase decreases with increased basicity as the silicate glass phase chemistry analyses (represented as icons) are positioned along the Olivine type liquid silicate glass-Monoxide phase boundary. This trend in liquid silicate compositions along the Monoxide phase boundary in the MnO-SiO_2-CaO-MgO-Al_2O_3 system have been shown in similar previous work (Olsen and Tangstad, 1995; Coetsee et al. 2017). This is also the trend observed in actual glass phases SEM analyses as presented in Figures 11, 17 and 19.

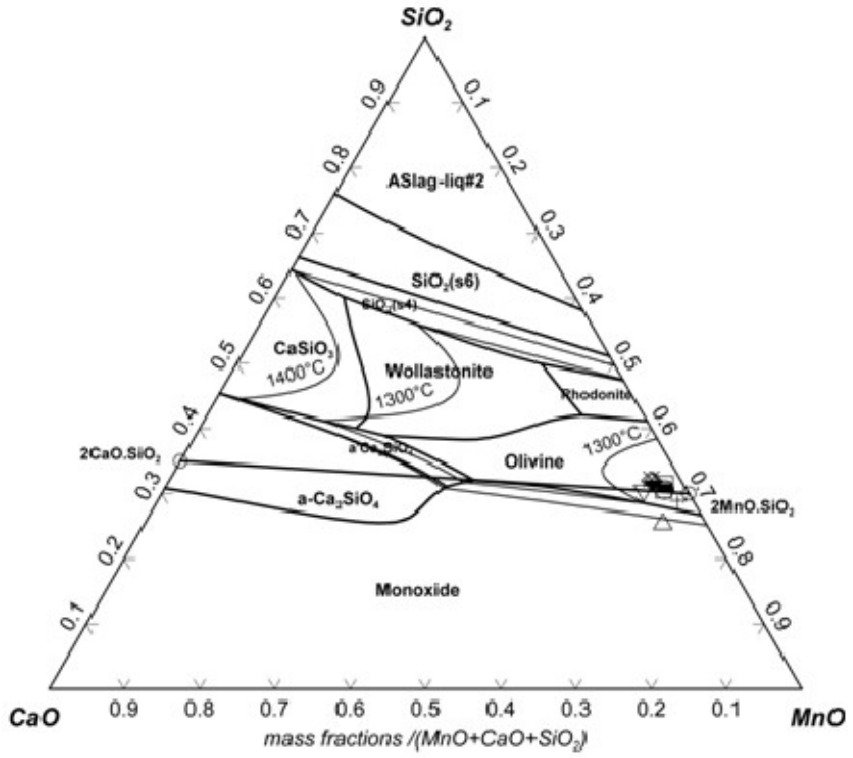

Figure 12: Glass phase chemistry SEM analyses points from Nchwaning ore sample reacted for 10 minutes at 1300°C plotted onto CaO-MnO-SiO_2-1%MgO-3%FeO pseudo-ternary phase diagram based on calculation inputs: Z=MnO+CaO+SiO_2, (g.MgO/g.Z) = 0.010 and (g.FeO/g.Z)=0.031

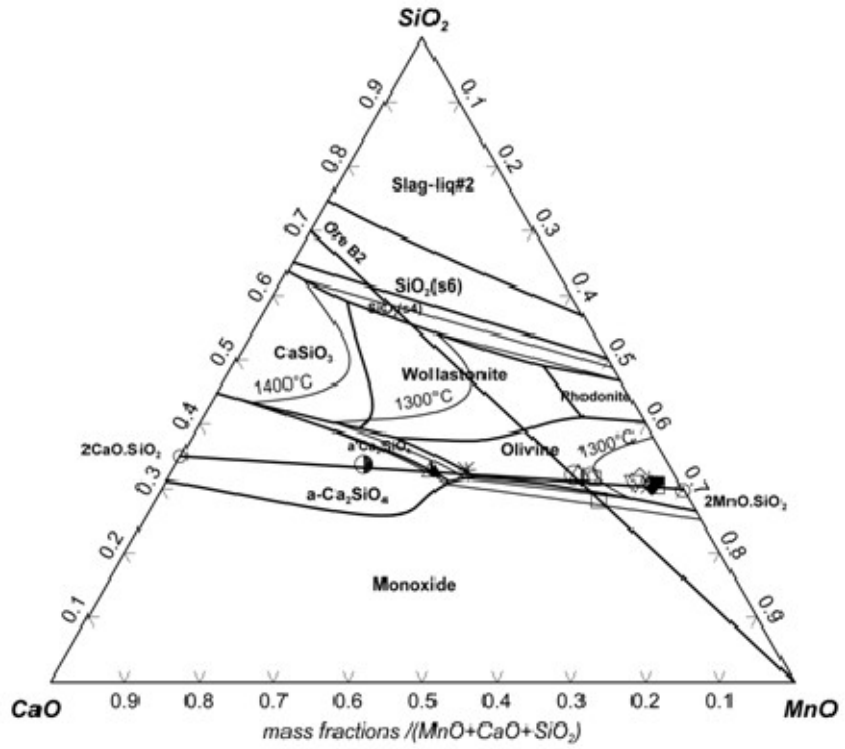

Figure 13: Glass phase chemistry SEM analyses points from Nchwaning ore sample reacted for 20 minutes (semi-filled icons) and 30 minutes at 1300°C plotted onto CaO-MnO-SiO_2-1%MgO-1%FeO pseudo-ternary phase diagram based on calculation inputs: Z=MnO+CaO+SiO_2, (g.MgO/g.Z) = 0.010 and (g.FeO/g.Z)=0.010

Figures 14-16 illustrate typical glass phase appearance within Mamatwan reduced ore particles. Similar to the phase morphology observed in Nchwaning ore, glass phase formation in Mamatwan ore occurred in association with monoxide phase, and mostly also in association with alloy phase areas. At 20 and 30 minutes reaction time the glass phase was typically devoid of iron oxide, whilst some iron oxide was still present in the glass phase at 10 minutes reaction time, up to 6 mass%. All glass phase compositions contained some MgO, with the highest level of 9%MgO measured at two points at 30 minutes reaction time. Glass phase compositions and their calculated liquidus temperatures are summarised in Table A.2. High basicity Mamatwan ore is expected to form less glass phase volume compared to the more acidic Wessels and Nchwaning ores since increased levels of MgO in the low FeO-CaO-MgO-MnO-SiO_2 system results in increased liquidus temperatures. At 10 minutes reaction time the relative quantity of glass phase observed was very low compared to 20 minutes reaction time.

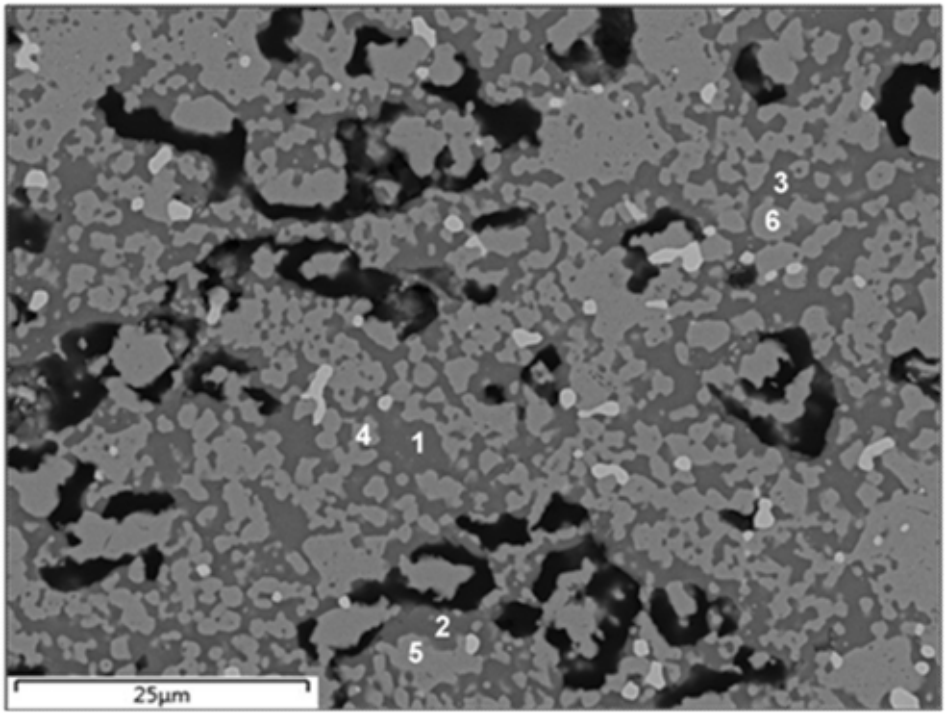

Figure 14: BSE image (x1600) of Mamatwan ore reacted for 10 minutes at 1300°C

	1	2	3	4	5	6
	glass	glass	glass	monoxide	monoxide	monoxide
CaO	32.0	29.5	26.7	3.6	1.7	1.6
FeO	2.1	6.2	2.0	5.0	5.0	5.0
MnO	29.9	29.1	38.3	81.5	86.0	88.2
SiO_2	31.5	29.3	28.3	0	0	0
MgO	4.6	5.8	4.6	6.2	7.3	5.2
Total	100	100	100	100	100	100
B2	1.02	1.01	0.94			
B3	1.16	1.20	1.11			
TL(°C)	1404	1467	>1500			

Table VIII: SEM analyses (mass%) of phases in Figure 14 for Mamatwan ore reacted for 10 minutes at 1300°C (TL=liquidus temperature)

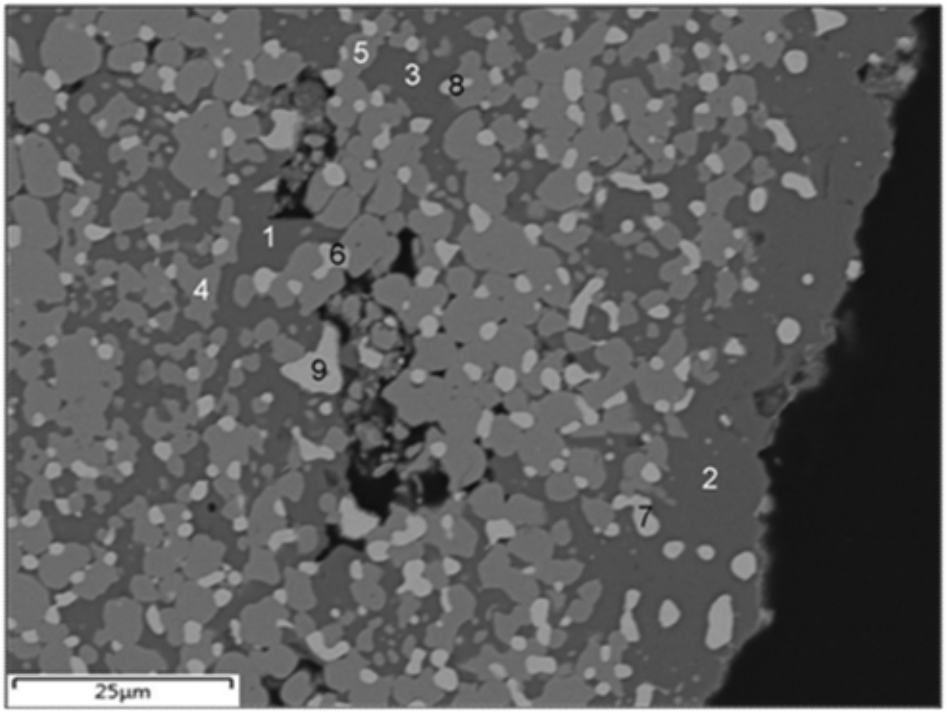

Figure 15: BSE image (x1200) of Mamatwan ore reacted for 20 minutes at 1300°C

	1	2	3	4	5	6	7	8	9
	glass	glass	glass	monoxide	monoxide	alloy	alloy	alloy	alloy
CaO	34.7	33.4	33.6	1.3	1.5				
FeO	1.0	0	2.6	9.9	1.2				
MnO	26.7	26.8	26.8	83.3	91.2				
SiO_2	33.1	34.0	32.4	0	0				
MgO	4.5	5.7	4.5	5.5	6.1				
Mn						7.1	8.2	7.6	7.8
Fe						92.9	91.8	92.4	92.2
Total	100	100	100	100	100	100	100	100	100
B2	1.0	1.0	1.0						
B3	1.2	1.2	1.2						
TL(°C)	1455	1382	1428						

Table IX: SEM analyses (mass%) of phases in Figure 15 for Mamatwan ore reacted for 20 minutes at 1300°C (TL=liquidus temperature)

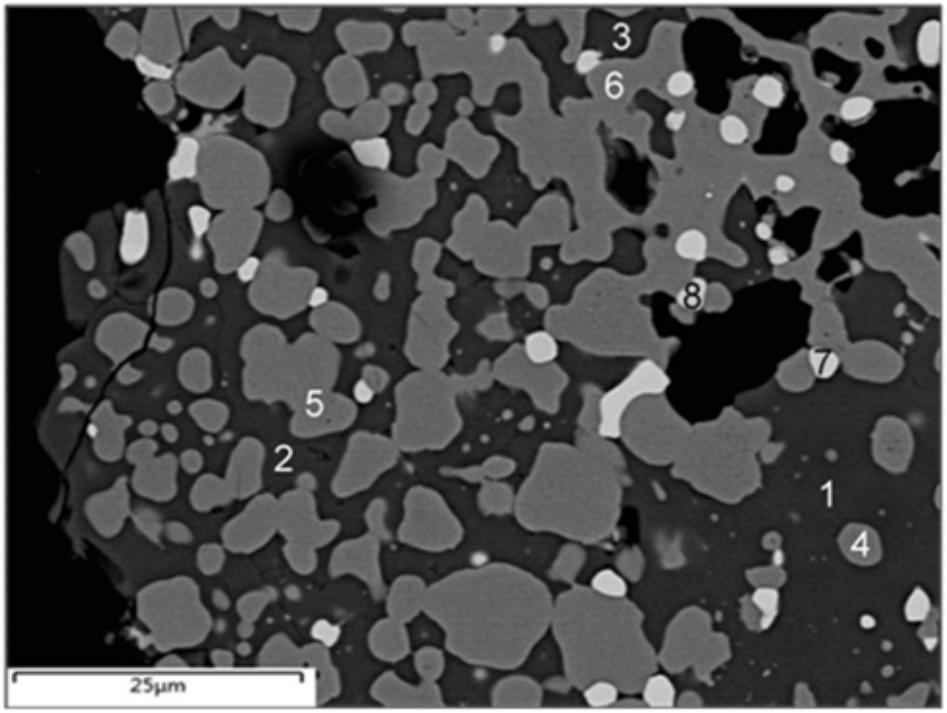

Figure 16: BSE image (x1600) of Mamatwan ore reacted for 30 minutes at 1300°C

	1	2	3	4	5	6	7	8
	glass	glass	glass	monoxide	monoxide	monoxide	alloy	alloy
CaO	33.2	33.9	53.9	1.9	1.4	1.6		
FeO	0	0	0	0	0	0		
MnO	23.2	22.5	9.2	84.3	83.2	84.5		
SiO_2	34.4	34.4	34.0	0	0	0		
MgO	9.3	9.2	2.9	13.8	15.4	13.9		
Mn							8.2	5.1
Fe							91.8	94.9
Total	100	100	100	100	100	100	100	100
B2	1.0	1.0	1.6					
B3	1.2	1.3	1.7					
TL(°C°)	1375	1386	>1500					

Table X: SEM analyses (mass%) of phases in Figure 16 for Mamatwan ore reacted for 30 minutes at 1300°C (TL=liquidus temperature)

Figure 17 provides a visualisation of glass phase composition changes with increased reaction time of Mamatwan ore. At 10 minutes reaction time the glass phase compositions fall in the two groups in terms of low basicity (1.1-1.2) and high MnO content (30-40%MnO) and high basicity (1.7-2.0) and low MnO content (10-20%MnO). Although the latter glass compositions appear to be fully molten in the SEM images, equilibrium calculations for these low MnO, high basicity compositions provide very high liquidus temperatures. These two separate groupings in glass composition displayed in Figure 17 can be explained to be due to incomplete chemical assimilation of calcined carbonate minerals, Kutnohorite and Calcite, into manganese containing silicate minerals of Braunite and Diopside. At 20 minutes reaction time a narrow range of MnO content and B3 values were measured in the glass phase areas (27-39 %MnO and 0.9-1.2 B3 values). Glass composition points for 30 minutes reaction time span the centre range of B3 values (1.1-1.7) between those of the high B3 grouping at 10

minutes and the 20 minutes glass compositions which were all of low basicity. A large proportion of glass phase analyses has low basicity values (B3<1.50) compared to the bulk ore basicity (B2=2.3 and B3=2.9, Table II).

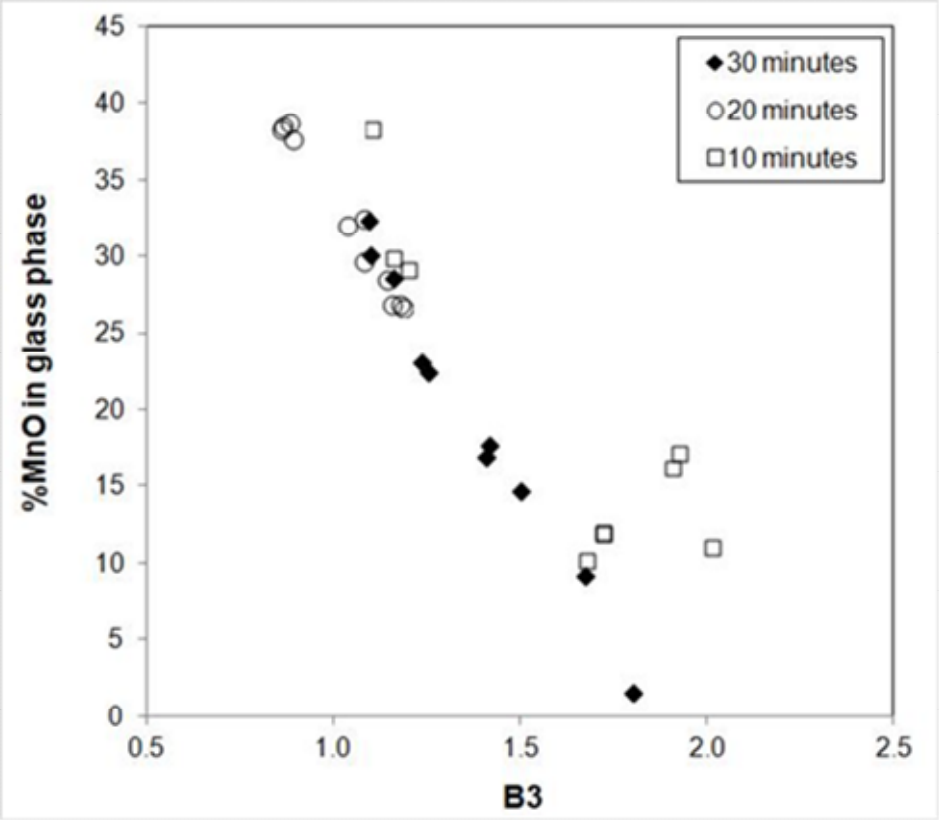

Figure 17: %MnO vs. B3 for glass phase compositions in Mamatwan ore reacted for 10, 20 and 30 minutes at 1300°C

The CaO-MnO-SiO_2-5%MgO phase diagram in Figure 18 contains the glass phase chemistry for Mamatwan ore reacted for 20 minutes at 1300°C, following adjustment of the analysed compositions to 5%MgO. The glass composition plots indicate higher basicity glass phase, compared to those of Nchwaning ore in Figure 13 because higher CaO content in Mamatwan ore results in high CaO content in the glass phase, whilst MgO mostly react with MnO to form monoxide phase, (Mn,Mg)O. Most of the glass composition points in Figure 18 are positioned between 1300°C and 1400°C, along the composition line between the $2CaO.SiO_2$ composition point and the $2MnO.SiO_2$ composition point. The reason for calculated glass phase liquidus temperatures above the experimental temperature of 1300°C is not clear. The glass phase areas analysed all appeared amorphous, as is illustrated in Figure 15. Few instances of of high levels of sulfur (3%S) or some barium contained in the glass were measured, but these were not the norm and does not account for the higher liquidus temperatures calculated compared to observed glass phase at 1300°C experimental temperature.

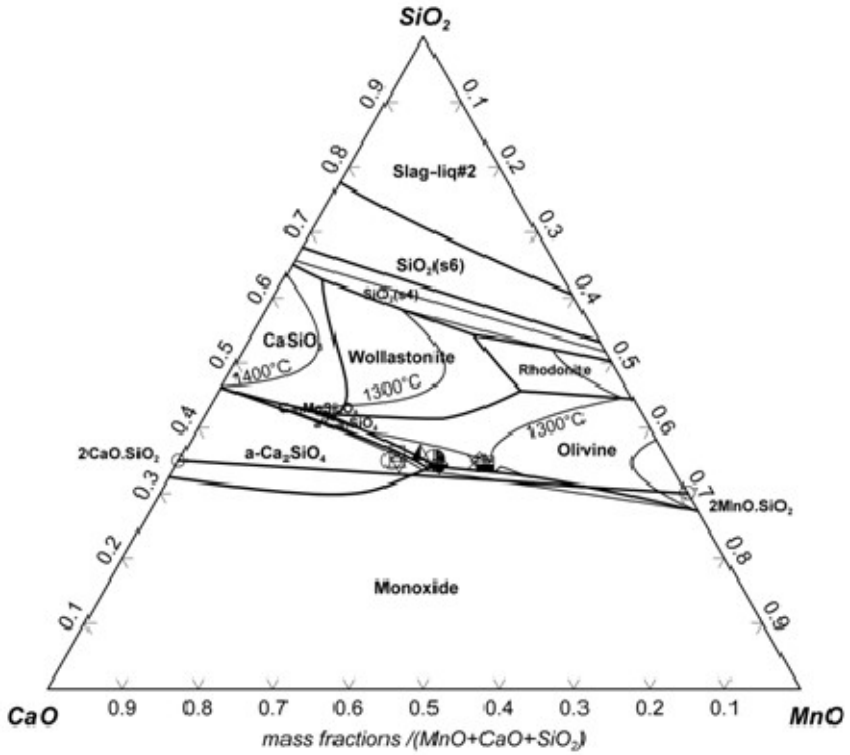

Figure 18: Glass phase chemistry SEM analyses points from Mamatwan ore sample reacted for 20 minutes at 1300°C plotted onto CaO-MnO-SiO_2-5%MgO pseudo-ternary phase diagram based on calculation inputs: Z=MnO+CaO+SiO_2, (g.MgO/g.Z) = 0.052 and (g.FeO/g.Z)=0

Glass phase basicity in Wessels reacted ore samples remained within a narrow range (0.6<B3<0.9) as displayed in Figure 19, compared to the trends in reacted Nchwaning ore (Figure 11) and Mammatwan ore (Figure 17). This narrow range of glass basicity values in notable because the Wessels ore basicity levels are relatively high at B2=1.8 and B3=1.9.

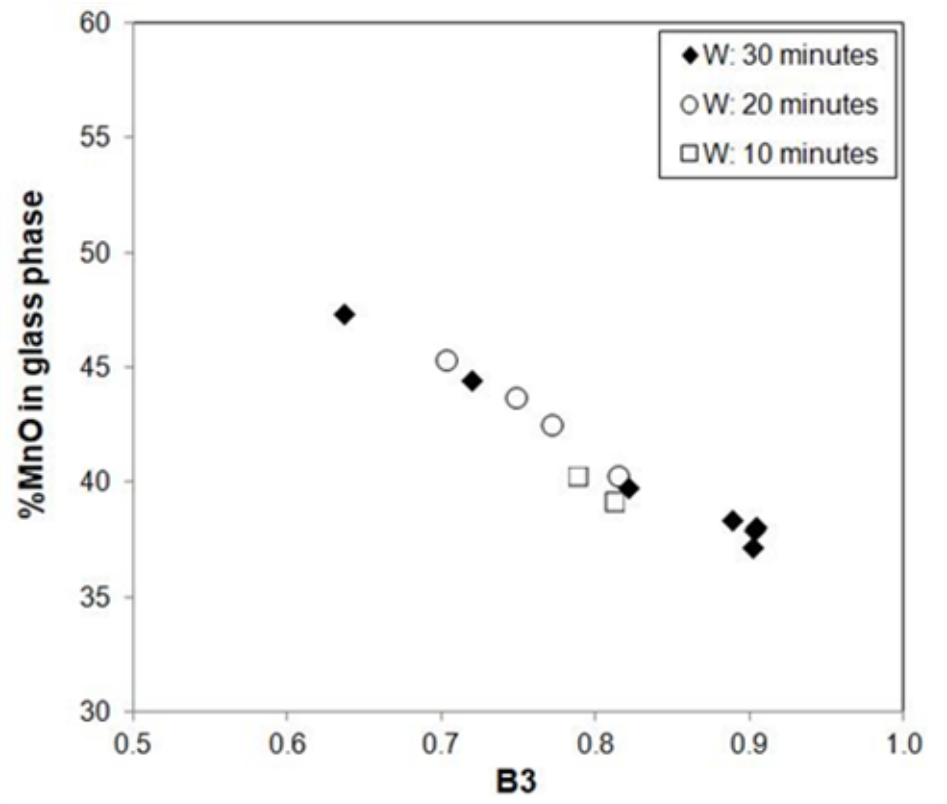

Figure 19: %MnO vs. B3 for glass phase compositions in Wessels ore reacted for 10, 20 and 30 minutes at 1300°C

Figures 20-22 illustrate typical glass phase appearance within Wessels reduced ore particles. Similar to Nchwaning and Mamatwan reduced ore, glass phase formation was mostly observed in association with monoxide phase. Due to the high sodium content in this ore sample, instances of large areas of early silicate glass phase formation were observed, even at 10 minutes reaction time. An initial sodium alumina silicate phase, see point 4 in Figure 20 (a), dissolved into into the matrix glass phase to lower the matrix glass phase liquidus temperature, see point 3 Figure 20 (a) and all the glass phase analyses in Figure 20 (b) glass phase areas.

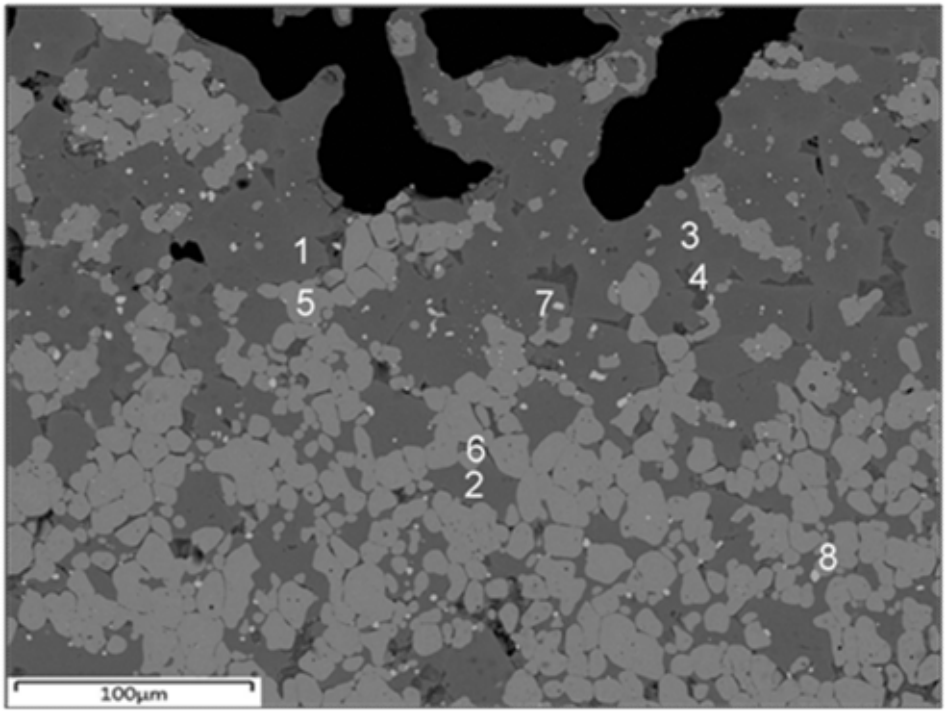

Figure 20 (a): BSE image (x330) of Wessels ore reacted for 10 minutes at 1300°C.

	1	2	3	4	5	6	7	8
	glass	glass	glass	glass	monoxide	monoxide	alloy	alloy
CaO	22.8	23.2	20.6	1.5	0.7	0.7		
FeO	0.9	0.9	0.7	2.3	3.7	3.0		
MnO	39.2	40.3	40.4	29.8	93.2	94.4		
SiO_2	33.0	32.9	33.2	38.5	0	0		
MgO	4.0	2.8	3.4	0.8	2.4	1.9		
Na_2O	0	0	1.4	22.8	0	0		
Al_2O_3	0	0	0.3	4.2				
Mn							2.7	3.5
Fe							97.3	96.5
Total	100	100	100	100	100	100	100	100
B2	0.69	0.70	0.62	0.04				
B3	0.81	0.79	0.72	0.06				
TL(°C)	1288	1273	1261	1104				

Table XI: SEM analyses (mass%) of phases in Figure 20 (a) for Wessels ore reacted for 10 minutes at 1300°C (TL=liquidus temperature)

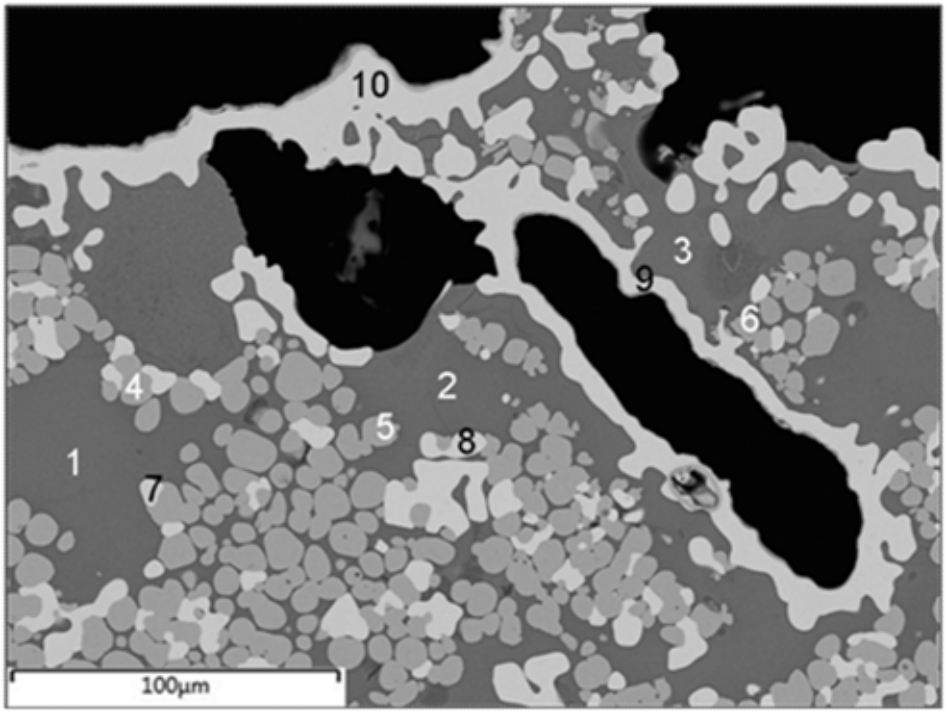

Figure 20 (b): BSE image of Wessels ore (x450) reacted for 10 minutes at 1300°C: sodium silicate glass formation.

	1	2	3	4	5	6	7	8	9	10
	glass	glass	glass	monoxide	monoxide	monoxide	alloy	alloy	alloy	alloy
CaO	19.8	19.3	18.8	0.5	0.5	0.5				
FeO	8.3	7.8	8.6	34.7	34.4	32.4				
MnO	22.9	22.0	24.2	60.3	60.6	62.5				
SiO_2	34.2	35.1	34.0	0	0	0				
MgO	1.9	2.1	2.3	4.5	4.5	4.6				
Na_2O	7.1	7.7	6.4	0	0	0				
Al_2O_3	5.7	5.9	5.7	0	0	0				
Mn							1.4	1.0	0.7	0.5
Fe							98.6	99.0	99.3	99.5
Total	100	100	100	100	100	100	100	100	100	100
B2	0.58	0.55	0.55							
B3	0.63	0.61	0.62							

Table XII: SEM analyses (mass%) of phases in Figure 20 (b) for Wessels ore reacted for 10 minutes at 1300°C

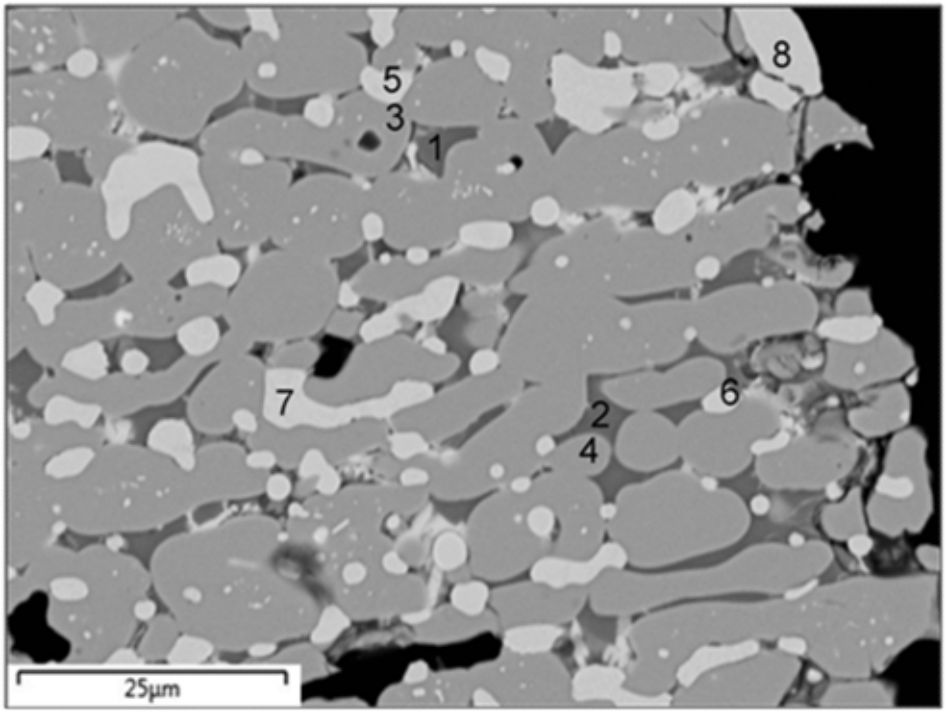

Figure 21: BSE image (x1100) of Wessels ore reacted for 20 minutes at 1300°C

	1	2	3	4	5	6	7	8
	glass	glass	monoxide	monoxide	alloy	alloy	alloy	alloy
CaO	22.0	23.8	0.3	0.4				
FeO	0.8	0.7	1.1	1.0				
MnO	45.4	43.7	98.9	98.6				
SiO_2	31.6	31.8	0	0				
MgO	0.3	0	0	0				
Mn					17.7	17.7	18.6	27.0
Fe					82.3	82.3	81.4	73.0
Total	100	100	100	100	100	100	100	100
B2	0.69	0.75						
B3	0.70	0.75						
TL(°C)	1241	1240						

Table XIII: SEM analyses (mass%) of phases in Figure 21 for Wessels ore reacted for 20 minutes at 1300°C (TL=liquidus temperature)

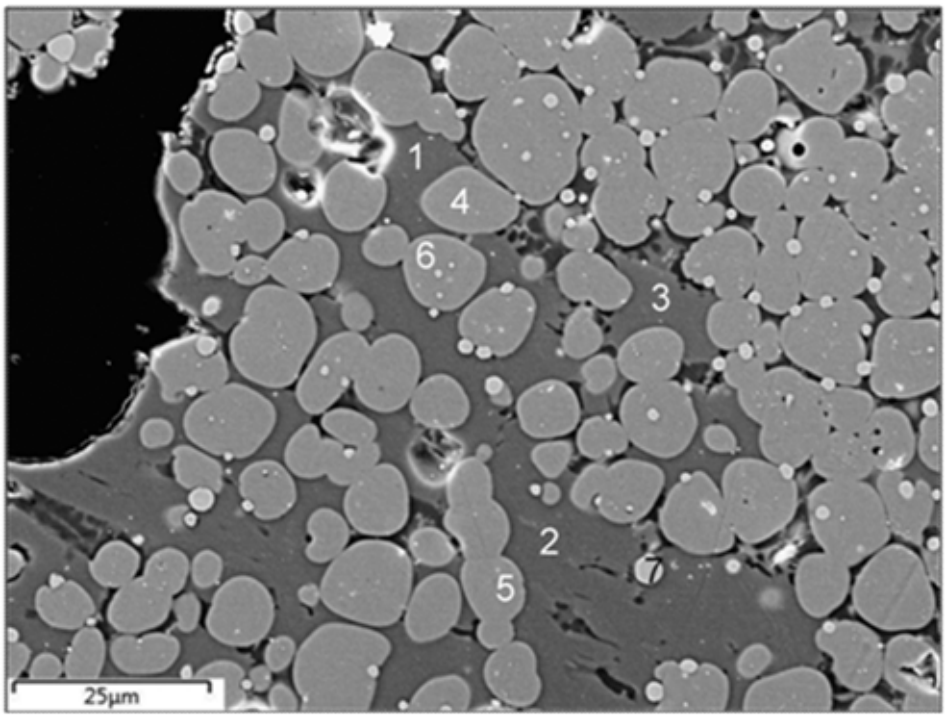

Figure 22: BSE image (x1500) of Wessels ore reacted for 30 minutes at 1300°C

	1	2	3	4	5	6	7
	glass	glass	glass	monoxide	monoxide	monoxide	alloy
CaO	21.6	25.4	18.9	0.7	0.7	0.9	
FeO	0	0	0	0	0.8	0	
MnO	44.5	39.8	47.4	98.0	97.2	97.7	
SiO_2	32.3	33.0	32.2	0	0	0	
MgO	1.6	1.7	1.5	1.3	1.3	1.4	
Mn							8.2
Fe							90.2
P							1.6
Total	100	100	100	100	100	100	100
B2	0.67	0.77	0.59				
B3	0.72	0.82	0.64				
TL(°C)	1258	1264	1266				

Table XIV: SEM analyses (mass%) of phases in Figure 22 for Wessels ore reacted for 30 minutes at 1300°C (TL=liquidus temperature)

In the glass matrix compositions for Wessels ore (not containing sodium) the low quantities (<1%) of MgO or FeO affect the glass phase liquidus temperatures by less than 5°C, therefore these glass phase compositions are projected onto the CaO-MnO-SiO_2 phase diagram in Figure 23. Glass compositions with higher levels of MgO (~2%) are displayed in the CaO-MnO-SiO_2-2%MgO diagram, Figure 24. The glass composition points in Figure 23 and Figure 24 are positioned onto or inside the 1300°C isotherm, well below the glass phase liquidus temperatures in the plots for Nchwaning and Mamatwan ores. In contrast to Nchwaning ore and Mamatwan ore in which the glass phase composition evolved in basicity and consequently the level of MnO in the glass phase as reaction time

increased, in Wessels ore the glass composition stayed within a narrow composition range along the $2CaO.SiO_2$-$2MnO.SiO_2$ composition line, irrespective the reaction time. This is most likely due to the smaller quantity of silicate minerals (Braunite II and Johannsenite) present in Wessels ore which is the source mineral of liquid silicate phase, whilst the rest of the mineral phases consist only of Mn and Fe oxides (Bixbyite, Hematite, Manganite) which will dissolve into the formed liquid silicate phase up to the MnO saturation level of the silicate glass phase at 1300°C. However, from Figures 23 and 24, it is clear that the liquid silicate phase is already close to its MnO saturation levels at 1300°C since the composition markers are placed on the Monoxide-silicate glass phase boundary.

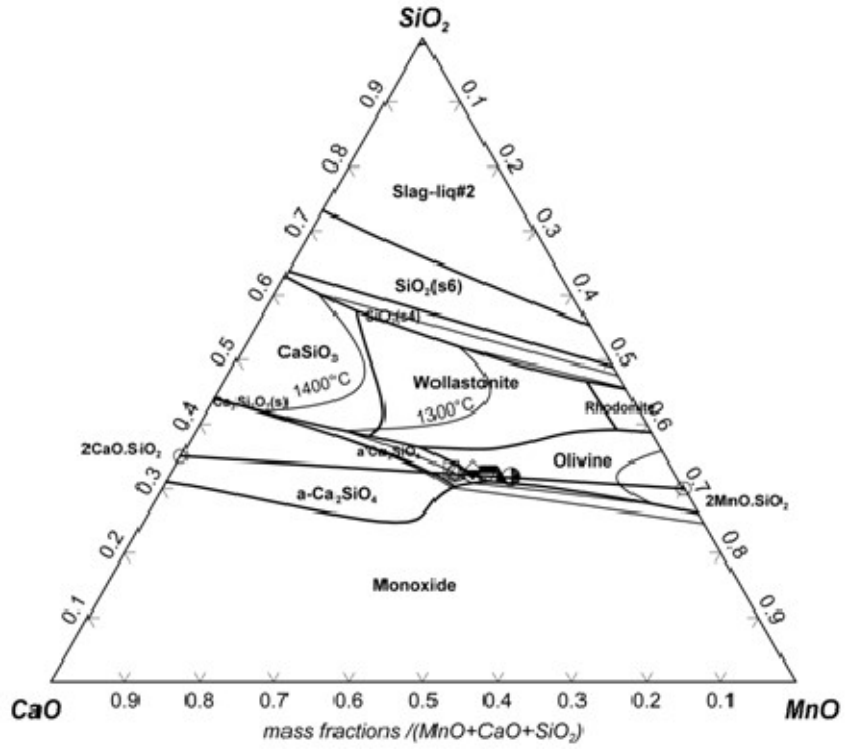

Figure 23: Glass phase chemistry SEM analyses points from Wessels ore sample reacted for 20 minutes (semi-filled icons) and 30 minutes (open icons) at 1300°C plotted onto CaO-MnO-SiO_2 ternary phase diagram.

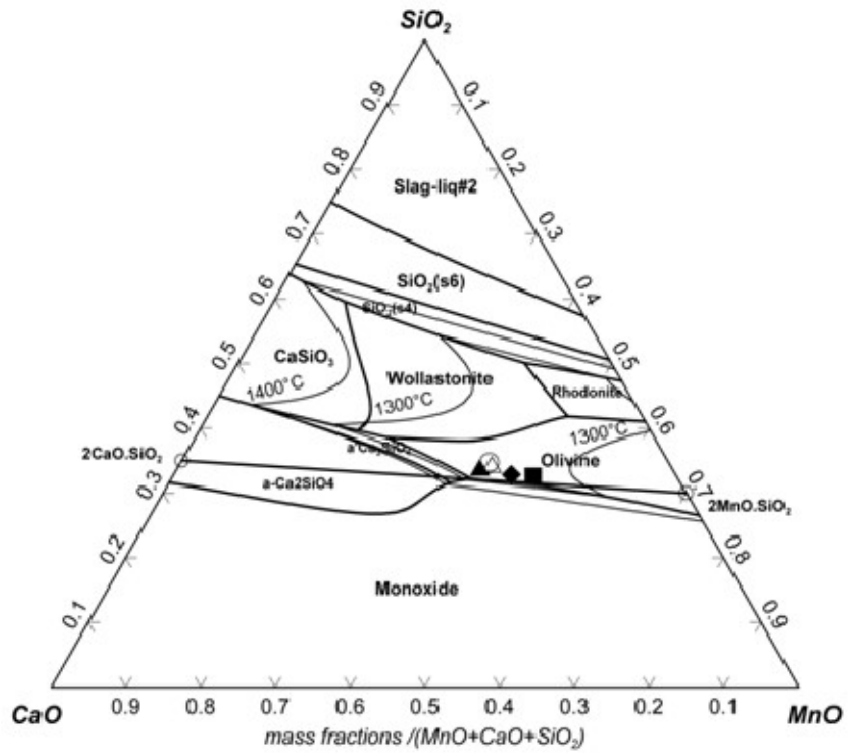

Figure 24: Glass phase chemistry SEM analyses points from Wessels ore sample reacted for 10 minutes (open icons) and 30 minutes (filled icons) at 1300°C plotted onto CaO-MnO-SiO_2-2%MgO pseudo-ternary phase diagram based on calculation inputs: Z=MnO+CaO+SiO_2, (g.MgO/g.Z) = 0.020 and (g.FeO/g.Z)=0

From the mineralogy data generated in the above analyses it is clear that low liquidus temperature matrix glass phases formed in all three South African manganese ore reacted samples: Nchwaning, Mamatwan and Wessels ore. This phenomenon is important in manganese ore smelting because the matrix glass phase formed at low temperatures will hinder CO gas access to the ore particle interior to reduce iron oxides to metallic iron, which is required to start reduction of manganese oxides positioned in contact with the metallic iron phases. Therefore, even though a particular ore contains high levels of iron oxide and associated manganese oxide in its mineral phases, if initial iron metallisation is hindered by glass matrix formation at low temperatures, then the ore will display a low reduction rate. The lowest matrix glass phase liquidus temperatures were calculated for Wessels ore. Qualitatively, both Wessels and Nchwaning ore formed more low temperature melting glass phase areas compared to Mamatwan ore.

4. Conclusions

- The crystal structures of the initial ore minerals in Nchwaning, Wessels and Mamatwan ores were almost completely absent from reduced ore XRD analyses following reaction for 10 minutes at 1300°C.

- Reduced ore particles consisted of three main phases: manganosite (Mn-Mg-monoxide), iron metal (containing up to 28 %Mn) and matrix silicate glass phase, even at short reaction times of 10 minutes at 1300°C.
- In all three manganese ores investigated (Nchwaning, Wessels and Mamatwan), silicate glass phase formed already at a relatively low reduction temperature of 1300°C.
- Initially formed silicate glass phase basicity levels were much lower than bulk ore basicity levels.
- The relative quantities of glass phase formation were higher in the acidic ores, Nchwaning ore and Wessels ore, compared to the extent of glass phase formation high basicity Mamatwan ore.
- Low liquidus temperature matrix glass phase formation lower manganese ore reduction rates by hindering CO gas access to the reduced ore particle interior where most of the iron oxides are reduced to metallic iron. The latter is required to start metallisation of manganese oxide phases in contact with iron metal prills.

Acknowledgements

The author appreciates contributions of Dr. Sabine Verryn (xrd Analytical & Consulting) for the XRD analyses and Mr. Dirk Odendaal (University of Pretoria) for polished section preparation and his assistance in completion of experiments. This work was supported by the University of Pretoria.

5. Appendix A

10 minutes	CaO	FeO	MnO	SiO_2	MgO	Total	B2	B3	LT (°C)[1]	PSP[2]
1	2.8	2.8	64.5	29.6	0.2	100	0.10	0.10	1326	Olivine
2	3.0	3.2	64.3	29.5	0.0	100	0.10	0.10	1320	Olivine
3	5.6	2.0	67.5	25.0	0.0	100	0.22	0.22	1409	Monoxide
4	5.8	1.6	62.7	29.8	0.0	100	0.20	0.20	1308	Olivine
5	3.9	3.6	61.1	30.6	0.8	100	0.13	0.15	1329	Olivine
6	3.8	3.6	61.0	30.8	0.8	100	0.12	0.15	1329	Olivine
7	3.6	5.3	60.6	30.1	0.3	100	0.12	0.13	1317	Olivine
8	3.3	4.9	61.1	30.3	0.3	100	0.11	012	1320	Olivine
9	2.3	4.8	62.7	29.9	0.4	100	0.10	0.10	1328	Olivine
10	2.1	5.2	65.3	26.9	0.5	100	0.10	0.10	1318	Olivine
20 minutes	CaO	FeO	MnO	SiO_2	MgO	Total	B2	B3	LT (°C)[1]	PSP[2]
1	3.2	0.9	65.7	30.2	0.0	100	0.11	0.11	1326	Olivine
2	3.9	0.0	65.6	30.5	0.0	100	0.13	0.13	1325	Olivine
3	1.4	4.5	62.1	29.9	2.2	100	0.05	0.12	1368	Olivine
4	1.1	5.0	61.2	30.4	2.3	100	0.03	0.11	1370	Olivine
5	17.9	1.0	36.3	33.6	11.1	100	0.53	0.86	1402	Olivine
6	18.9	1.6	37.6	33.1	8.8	100	0.57	0.84	1364	Olivine
7	32.4	0.0	34.9	32.7	0.0	100	0.99	0.99	1364	a'Ca_2SiO_4
8	41.0	0.0	25.2	33.7	0.0	100	1.22	1.22	1604	a'Ca_2SiO_4
30 minutes	CaO	FeO	MnO	SiO_2	MgO	Total	B2	B3	LT (°C)[1]	PSP[2]
1	13.4	0.0	53.8	31.8	1.0	100	0.42	0.45	1287	Olivine
2	12.0	1.0	58.5	27.6	0.9	100	0.43	0.47	1361	Monoxide
3	12.5	1.0	53.9	31.5	1.0	100	0.40	0.43	1289	Olivine
4	4.9	0.0	62.1	31.1	1.9	100	0.16	0.22	1352	Olivine
5	3.7	0.8	62.8	30.5	2.2	100	0.12	0.19	1362	Olivine
6	5.9	0.8	62.2	30.7	0.4	100	0.19	0.20	1318	Olivine
7	4.3	0.0	64.6	30.4	0.7	100	0.14	0.16	1334	Olivine
8	27.4	0.8	39.0	32.4	0.3	100	0.85	0.86	1251	a'Ca_2SiO_4
9	27.5	0.0	39.8	32.3	0.4	100	0.85	0.86	1260	a'Ca_2SiO_4
10	11.3	0.0	55.7	31.6	1.4	100	0.36	0.40	1305	Olivine
11	10.9	0.0	56.5	31.1	1.5	100	0.35	0.40	1308	Olivine

1: LT(°C)=Liquidus Temperature; 2: PSP=Primary solidification phase

Table A.I: SEM-EDS analyses of glass phases in Nchwaning reduced ore particles (mass%)

10 minutes	CaO	FeO	MnO	SiO_2	MgO	Total	B2	B3	LT (°C)[1]	PSP[2]
1	32.0	2.1	29.9	31.5	4.6	100	1.02	1.16	1404	a-Ca_2SiO_4
2	29.5	6.2	29.1	29.3	5.8	100	1.01	1.20	1467	Monoxide
3	26.7	2.0	38.3	28.3	4.6	100	0.94	1.11	>1500	Monoxide
4	49.9	3.9	11.1	28.2	7.0	100	1.77	2.02	>1600	a-Ca_2SiO_4
5	51.1	3.8	16.3	27.5	1.4	100	1.86	1.91	>1600	a-Ca_2SiO_4
6	48.9	3.3	17.2	27.2	3.5	100	1.80	1.93	>1600	a-Ca_2SiO_4
7	52.9	0.0	12.0	32.3	2.8	100	1.64	1.72	>1600	a-Ca_2SiO_4
8	53.5	0.0	12.0	32.4	2.2	100	1.65	1.72	>1600	a-Ca_2SiO_4
9	53.7	0.0	10.2	33.6	2.6	100	1.60	1.68	>1600	a-Ca_2SiO_4
20 minutes	CaO	FeO	MnO	SiO_2	MgO	Total	B2	B3	LT (°C)[1]	PSP[2]
1	34.7	1.0	26.7	33.1	4.5	100	1.05	1.18	1455	a-Ca_2SiO_4
2	33.4	0.0	26.8	34.0	5.7	100	0.98	1.15	1382	a-Ca_2SiO_4
3	33.6	2.6	26.8	32.4	4.5	100	1.04	1.18	1428	a-Ca_2SiO_4
4	23.9	0.0	38.2	33.3	4.6	100	0.72	0.86	1297	Olivine
5	34.9	0.0	28.4	33.5	3.2	100	1.04	1.14	1448	a-Ca_2SiO_4
6	23.1	0.0	38.5	33.0	5.4	100	0.70	0.86	1306	Olivine
7	24.5	0.0	37.6	33.1	4.8	100	0.74	0.89	1302	Olivine
8	23.2	0.0	38.8	32.6	5.4	100	0.71	0.88	1307	Olivine
9	29.3	0.0	32.0	33.4	5.3	100	0.88	1.03	1320	Olivine
10	30.5	0.0	29.7	33.8	6.0	100	0.90	1.08	1331	Olivine
11	28.8	1.0	32.5	32.0	5.7	100	0.90	1.08	1338	Monoxide
30 minutes	CaO	FeO	MnO	SiO_2	MgO	Total	B2	B3	LT (°C)[1]	PSP[2]
1	33.2	0.0	23.2	34.4	9.3	100	0.96	1.23	1375	Olivine
2	33.9	0.0	22.5	34.4	9.2	100	0.98	1.25	1386	a-Ca_2SiO_4
3	53.9	0.0	9.2	34.0	2.9	100	1.59	1.67	>1600	a-Ca_2SiO_4
4	34.0	0.0	30.1	33.3	2.5	100	1.02	1.10	1420	a-Ca_2SiO_4
5	32.6	0.0	32.4	32.3	2.6	100	1.01	1.09	1410	a-Ca_2SiO_4
6	36.2	0.0	28.6	33.1	2.1	100	1.10	1.16	1500	a-Ca_2SiO_4
7	45.5	0.0	17.8	34.1	2.7	100	1.34	1.41	>1600	a-Ca_2SiO_4
8	46.1	0.0	17.0	34.5	2.3	100	1.34	1.40	>1600	a-Ca_2SiO_4
9	49.4	0.0	14.7	34.2	1.7	100	1.45	1.50	>1600	a-Ca_2SiO_4
10	63.2	0.0	1.6	35.2	0.0	100	1.80	1.80	>1600	a-Ca_2SiO_4

1: LT(°C)=Liquidus Temperature; 2: PSP=Primary solidification phase

Table A.2: SEM-EDS analyses of glass phases in Mamatwan reduced ore particles (mass%)

10 minutes	CaO	FeO	MnO	SiO_2	MgO	Total	B2	B3	LT (°C)[1]	PSP[2]
1	22.8	0.9	39.2	33.0	4.0	100	0.69	0.81	1288	Olivine
2	23.2	0.9	40.3	32.9	2.8	100	0.70	0.79	1273	Olivine
20 minutes	CaO	FeO	MnO	SiO_2	MgO	Total	B2	B3	LT (°C)[1]	PSP[2]
1	25.0	0.0	42.5	32.4	0.0	100	0.77	0.77	1241	Olivine
2	26.8	0.0	40.3	32.9	0.0	100	0.81	0.81	1243	Olivine
3	22.0	0.8	45.4	31.6	0.3	100	0.69	0.70	1241	Olivine
4	23.8	0.7	43.7	31.8	0.0	100	0.75	0.75	1240	Olivine
30 minutes	CaO	FeO	MnO	SiO_2	MgO	Total	B2	B3	LT (°C)[1]	PSP[2]
1	29.1	0.0	38.1	32.5	0.3	100	0.89	0.90	1291	a'Ca_2SiO_4
2	29.4	0.0	37.2	33.0	0.4	100	0.89	0.90	1284	a'Ca_2SiO_4
3	21.6	0.0	44.5	32.3	1.6	100	0.67	0.72	1258	Olivine
4	25.4	0.0	39.8	33.0	1.7	100	0.77	0.82	1264	Olivine
5	18.9	0.0	47.4	32.2	1.5	100	0.59	0.64	1266	Olivine
6	28.3	0.0	38.4	32.4	0.4	100	0.87	0.89	1274	a'Ca_2SiO_4
7	29.0	0.0	38.0	32.6	0.4	100	0.89	0.90	1287	a'Ca_2SiO_4

1: LT(°C)=Liquidus Temperature; 2: PSP=Primary solidification phase

Table A.3: SEM-EDS analyses of glass phases in Wessels reduced ore particles (mass%)

6. References

Akdogan, G., Eric, R.H., 1995. Kinetics of the solid-state carbothermic reduction of Wessel manganese ores. *Metallurgical and Materials Transactions B*, Vol.26B, pp.13-24.

ASTM A99-03(2014), Standard Specification for Ferromanganese, ASTM International, West Conshohocken, PA, 2014, www.astm.org

Braga, R.S., Takano, C., Mourao, M.B., 2007. Prereduction of self-reducing pellets of manganese ore. *Ironmaking and Steelmaking*, Vol.34, pp.279-284.

Chetty, D., Gutzmer, 2018. Quantitative mineralogy to address energy consumption in smelting of ores from the Kalahari Manganese Field, South Africa. *INFACON XV, The Fifteenth International Ferroalloys Congress*, Cape Town, South Africa, 25-28 February.

Coetsee, T., Reinke, C., Nell, J., Pistorius, P.C., 2015. Reduction mechanisms in manganese ore reduction. *Metallurgical and Materials Transactions B*, Vol. 46B, pp. 2534-2552.

Coetsee, T., Nell, J., Pistorius, P.C., 2017. Phase characterization of high basicity manganese slags. *Metallurgical and Materials Transactions B*, Vol.48B, pp.1463-1485.

Coetsee, T., 2018. MnO reduction in high carbon ferromanganese production: practice and theory. *Mineral Processing and Extractive Metallurgy Review*, Vol.39, pp. 351-358.
DOI: 10.1080/08827508.2018.1459618

Eric, R.H., Burucu, E., 1992. The mechanism and kinetics of the carbothermic reduction of Mamatwan manganese ore fines. *Minerals Engineering*, Vol.5, pp.795-815.

Kleyenstüber, A.S.E., 1984. The mineralogy of the Manganese-bearing Hotazel formation, of the Proterozoic Transvaal sequence in Griqualand West, South Africa. Transactions of the Geological Society of South Africa, Vol. 87, pp. 257-272.

Koursaris, A., Kleyenstüber, A.S.E., Finn, C.W.P., 1983. A mineralogical investigation of the reduction of Mamatwan manganese ore with carbon. *Special Publication, Geological Society of South Africa*, Vol.7, pp.375-382.

Koursaris, A., See, J.B., 1979. Reactions in the production of high-carbon ferromanganese from Mamatwan ore. *Journal of the South African Institute of Mining and Metallurgy*, Vol.79, pp. 149-158.

Liu, B., Zhang, Y., Su, Z., Lu, M., Li, G., Jiang, T., 2018. A study on the carbonization and alloying process of MnO_2 by methane-hydrogen gas mixture in the presence of Fe_2O_3. Powder Technology, Vol. 325, pp. 271-279.

Liu, B., Zhang, Y., Lu, M., Su, Z., Li, G., Jiang, T., 2019. Extraction and separation of manganese and iron from ferruginous manganese ores: A review. *Minerals Engineering*, Vol. 131, pp. 286-303.

Olsen, S.E., Tangstad, M., 1995. The imposrtance of slag basicity in the production of high carbon ferromanganese. 53rd Electric Furnace Conference, Orlando, USA, pp. 93-98.

Ostrovski, O. I., Anacleto, N., Ganguly, S., 2004. Reduction of manganese ores by methane-containing gas. *INFACON X, Tenth International Ferroalloys Congress*, Cape Town, South Africa, 1-4 February, pp. 173-183.

Ostrovski, O. I., Webb, T.J.M., 1995. Reduction of siliceous manganese ore by graphite. *ISIJ International*, Vol.35, pp.1331-1339.

Rankin, W.J., Van Deventer, J.S.J., 1980. The kinetics of the reduction of manganous oxide by graphite. *Journal of the South African Institute of Mining and Metallurgy*, Vol. 80, pp. 239-247.

Slag Atlas, Verlag Stahleisen GmbH, Düsseldorf, 1995, p. 90.

Tangstad, M., Olsen, S.E., 1997. Phase relations in ferromanganese slags during melting and reduction. *5th International Conference on Molten Slags, Fluxes and Salts*, ISS, Warrendale, pp.549-555.

Van Deventer, J.S.J., 1987. The effect of gangue components on the reduction of manganosite by graphite: An isothermal kinetic study.*Thermochimica Acta*, Vol. 112, pp. 365-377.

Zhang, Y., Liu, B, Zhixiong, Y., Su, Z., Luo, W., Li, G., Jiang, T., 2016. Consolidation behavior of high-Fe manganese ore sinters with natural basicity. *Mineral Processing and Extractive Metallurgy Review*, Vol.37, pp. 333-341.